D12.4 Technical handbook for resilient structural systems

MULTICARE

Funded by
the European Union

D12.4 Technical handbook for resilient structural systems

Dissemination Level: PU - Public
Lead Partner: UNIROMA1
Due date: 30 September 2025
Actual submission date: 1 October 2025

PUBLISHED IN THE FRAMEWORK OF

MULTICARE (Horizon Europe grant 101123467)

AUTHORS

Simone D'Amore (UNIROMA1)
Giada Formichetti (UNIROMA1))
Livio Pedone (UNIROMA1)
Stefano Pampanin (UNIROMA1)

REVISION AND HISTORY CHART

VERSION	DATE	EDITORS	COMMENT
V0.1	20 September 2025	Simone D'Amore (UNIROMA1) Giada Formichetti (UNIROMA1) Leonardo Silvestri (UNIROMA1)	Draft
V0.1	25 September 2025	Carmine Molitierno (UNINA)	Revision
V0.2	30 September 2025	Simone D'Amore (UNIROMA1) Giada Formichetti (UNIROMA1)	Final Document

DISCLAIMER

The information in this document is subject to change without notice. Company or product names mentioned in this document may be trademarks or registered trademarks of their respective companies.

Funded by the European Union

This project has received funding from the European Union under the Horizon Europe Research & Innovation Programme (Grant Agreement no. 101123467 MultiCare). Views and opinions expressed are however those of author(s) only and do not necessarily reflect those of the European Union. Neither the European Union nor the granting authority can be held responsible for them.

Table of contents

Funded by the European Union

This project has received funding from the European Union under the Horizon Europe Research & Innovation Programme (Grant Agreement no. 101123467 MultiCare). Views and opinions expressed are however those of author(s) only and do not necessarily reflect those of the European Union. Neither the European Union nor the granting authority can be held responsible for them.

LIST OF FIGURES

Funded by the European Union

This project has received funding from the European Union under the Horizon Europe Research & Innovation Programme (Grant Agreement no. 101123467 MultiCare). Views and opinions expressed are however those of author(s) only and do not necessarily reflect those of the European Union. Neither the European Union nor the granting authority can be held responsible for them.

Funded by the European Union

This project has received funding from the European Union under the Horizon Europe Research & Innovation Programme (Grant Agreement no. 101123467 MultiCare). Views and opinions expressed are however those of author(s) only and do not necessarily reflect those of the European Union. Neither the European Union nor the granting authority can be held responsible for them.

LIST OF TABLES

Funded by the European Union

This project has received funding from the European Union under the Horizon Europe Research & Innovation Programme (Grant Agreement no. 101123467 MultiCare). Views and opinions expressed are however those of author(s) only and do not necessarily reflect those of the European Union. Neither the European Union nor the granting authority can be held responsible for them.

1. Introduction

1.1. MULTICARE project

The built environment is ill-prepared for more frequent and increasingly intense climate-related extreme events. The current building stock is particularly vulnerable because it has limited or no capacity to adapt and recover from extreme events thereby leading to building failures that cause severe socio-economic losses and adversely affecting the health and wellbeing of people. Recent scientific and technological advances in the construction industry provide timely solutions for improving the resilience for specific single hazards (e.g. flood hazard or seismic hazard), but they are often not cost effective, rarely eco-friendly and nearly never address the multiple hazards present in many locations. This is hardly surprising because there is neither a clearly defined framework for quantifying the whole-life socio-economic-environmental impacts of extreme natural events nor tools for assessing the holistic climate resilience of buildings. Consequently, it is currently very challenging to develop/select optimal solutions for real-world multi-hazard scenarios.

MULTICARE will address this challenge directly by developing new multi-criteria decision-support frameworks and providing plug & play technological and digital solutions for improving the resilience of the built environment in a cost-effective, reliable and sustainable manner. The technological solutions consist of multi-functional low-carbon resilient technologies embedded in modular and prefabricated construction for the next generation of high performance and smart buildings, characterized by enhanced safety, energy efficiency, environmental-sustainability, improved quality of life, circularity, and scalability for a broad range of natural events and end-user. The plug & play technologies will be applied to either new multi-story buildings or existing structures by means of low-invasive external interventions. The digital solutions consist of a suite of multi-disciplinary digital services and tools for performing multi-hazard resilience assessment, design, operation and management across multiple scales (material, component, building, neighborhood/city). The new digital tools will enable stakeholders to make informed decisions in the selection of materials/solutions, including for heritage buildings, and support resilient supply chains. The effectiveness of the MULTICARE solutions will be demonstrated through large-scale pilots (3 buildings, 4 neighborhoods/district) in three different European countries carefully selected for their diverse local environmental, social and economic conditions (Italy, Netherlands, Romania). Banks and institutional investors will be engaged to better understand the financial risk reduction value of resilience and update existing and future “green finance” mechanisms that will help to leverage the project results. A user-center, inclusive and participatory approach will be consistently implemented throughout the project to engage citizens and extend the durability of MULTICARE impact.

To achieve these ambitious goals, MULTICARE brings together a unique interdisciplinary Consortium of 21 partners (Table 1) from 6 different EU countries with strong R&D and practical expertise, who are either established leaders in their sector or agile SMEs in emerging fields. Altogether the Consortium members span across the whole technical and

Funded by the European Union

This project has received funding from the European Union under the Horizon Europe Research & Innovation Programme (Grant Agreement no. 101123467 MultiCare). Views and opinions expressed are however those of author(s) only and do not necessarily reflect those of the European Union. Neither the European Union nor the granting authority can be held responsible for them.

value chain required for developing and implementing solutions in terms of design, digitization, manufacturing, construction and monitoring of resilient and sustainable buildings. The Consortium also includes partners with experience in social sciences, user engagement, and training to ensure the success and widespread application of new technologies in local communities. The Consortium will also support clustering activities with other relevant research projects to share knowledge and raise public awareness of building resilience. An international outreach and cooperation strategy will also be implemented to tackle the project challenges.

Table 1. Consortium

Number	Role	Short Name	Legal Name	Country
1	CO	TU Delft	TECHNISCHE UNIVERSITEIT DELFT	NL
2	BEN	PFE	PRIEDEMANN FASSADENBERATUNG GMBH	DE
3	BEN	IES R&D	IES R&D	IE
4	BEN	INCDFP	INSTITUTUL NATIONAL DE CERCETARE-DEZVOLTARE PENTRU FIZICA PAMANTULUI	RO
5	BEN	UNIROMA1	UNIVERSITA DEGLI STUDI DI ROMA LA SAPIENZA	IT
6	BEN	XLD	X-LAM DOLOMITI SRL	IT
7	BEN	STRESS	SVILUPPO TECNOLOGIE E RICERCA PER L'EDILIZIA SISMICAMENTE SICURA ED ECOSOSTENIBILE SCARL	IT
7.1	AE	UNINA	UNIVERSITA DEGLI STUDI DI NAPOLI FEDERICO II	IT
8	BEN	AMS Institute	STICHTING AMSTERDAM INSTITUTE FORADVANCED METROPOLITAN SOLUTIONS(AMS)	NL
9	BEN	PMB	MUNICIPIUL BUCURESTI	RO
10	BEN	ASM	ASM - CENTRUM BADAN I ANALIZ RYNKUSPOLKA Z OGRANICZONA ODPOWIEDZIALNOSCIA	PL
11	BEN	RoGBC	ASOCIATIA ROMANIA GREEN BUILDING COUNCIL	RO
12	BEN	RINA-C	RINA CONSULTING SPA	IT
13	BEN	UTBV	UNIVERSITATEA TRANSILVANIA DIN BRASOV	RO
14	BEN	ACER	AGENZIA CAMPANA PER L EDILIZIA RESIDENZIALE	IT
15	BEN	Boom	BOOM BUILDS B.V.	NL
16	BEN	OMRT	OMRT BV	NL
17	BEN	ROTHO BLAAS SRL	ROTHO BLAAS SRL	IT
18	BEN	ARUP	ARUP BV	NL
19	BEN	Tecuci	MUNICIPIUL TECUCI	RO
20	BEN	Hölscher	DIPL.-ING. HPLSCHER GMBH & CO.KG	DE

1.2. Deliverable

As per Grant Agreement, deliverable 12.4 will provide guidelines for designing low-damage connections and structural systems that are easy to assemble and disassemble, maintain and re-use. It also provides alternative low-damage detailing.

Funded by the European Union

This project has received funding from the European Union under the Horizon Europe Research & Innovation Programme (Grant Agreement no. 101123467 MultiCare). Views and opinions expressed are however those of author(s) only and do not necessarily reflect those of the European Union. Neither the European Union nor the granting authority can be held responsible for them.

Table 2. Key deliverable information. Source: MULTICARE Grant Agreement.

Deliverable number and name	Work Package n°	Lead Beneficiary	Type
D12.4 – Technical handbook for resilient structural systems	WP12	5 – UNIROMA1	R – Document, report

2. Low-Damage resilient structural systems

2.1. Post-tensioned structures

The growing challenges posed by catastrophic events, together with the well-documented vulnerability of modern "code-conforming" buildings observed in recent earthquakes, underscore the urgent need for advanced technological solutions in the building sector. To this end, recent research efforts within the earthquake engineering community are focusing on advanced seismic protection technologies to enhance the resilience of the built environment, also promoting sustainability through the use of low-carbon materials such as timber. Within this context, rocking structural systems equipped with internal post-tensioning cables or tendons have emerged as a particularly effective technology, enabling a damage-control philosophy that limits structural damage during seismic events. The origins of this low-damage structural system can be traced back to the 1990s, when it was first introduced through the US-PRESSS (PREcast Seismic Structural System) program, led by Professor Nigel Priestley at the University of California, San Diego (Priestley, 1991; Priestley et al., 1999). The project aimed to develop a high-performance and cost-effective solution able to withstand severe earthquakes with negligible damage. This new structural system replaces the conventional plastic hinge (Figure 1a) - which can be deemed not cost-effective to repair, often consequently leading to building demolition (Pampanin, 2012; 2015) – with a controlled "rocking and dissipative" mechanism at the interface between the dry-jointed structural members (i.e., beam-to-column, column-to-foundation, and wall-to-foundation connections). Unbonded post-tensioned tendons/bars are provided, running throughout the beams, columns, and walls. This reinforcement is designed to remain elastic, allowing the closure of the pre-existing gap between the members at the end of the earthquake-induced rocking motion. Additionally, internal mild steel or external fuse-type replaceable "Plug&Play" dissipaters can also be included (Figure 1b), this way enabling energy dissipation. Of the two latter solutions, the Plug&Play dissipaters are of particular interest for their ease of installation, inspection from outside, and replaceability, as they are the only elements to get damaged after the earthquake. This way, the equivalence between ductility and damage, necessary to ensure life-safety, can be avoided.

Funded by the European Union

This project has received funding from the European Union under the Horizon Europe Research & Innovation Programme (Grant Agreement no. 101123467 MultiCare). Views and opinions expressed are however those of author(s) only and do not necessarily reflect those of the European Union. Neither the European Union nor the granting authority can be held responsible for them.

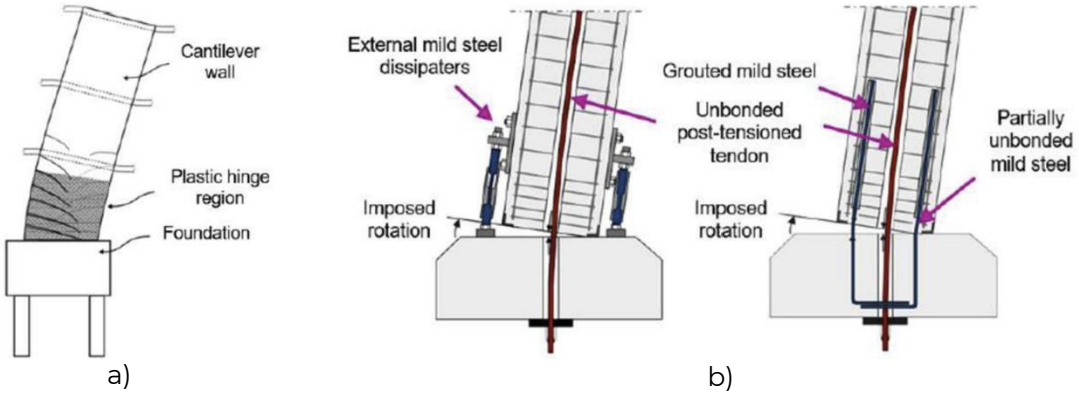

Figure 1. a) Traditional plastic hinge in a monolithic structure (modified after fib, 2003); b) Hybrid connections of the PRESSS structural system, with external Plug&Play dissipaters on the left, and internal mild steel bars on the right (modified after Marriott et al., 2008).

As shown in Figure 2, the Plug&Play dissipaters consist of axial tension-compression yielding mild steel bar with a reduced fuse-type section where plastic deformations are concentrated. To allow for their yielding in compression, these devices are inserted within an anti-buckling steel tube filled with grout or, even better, epoxy.

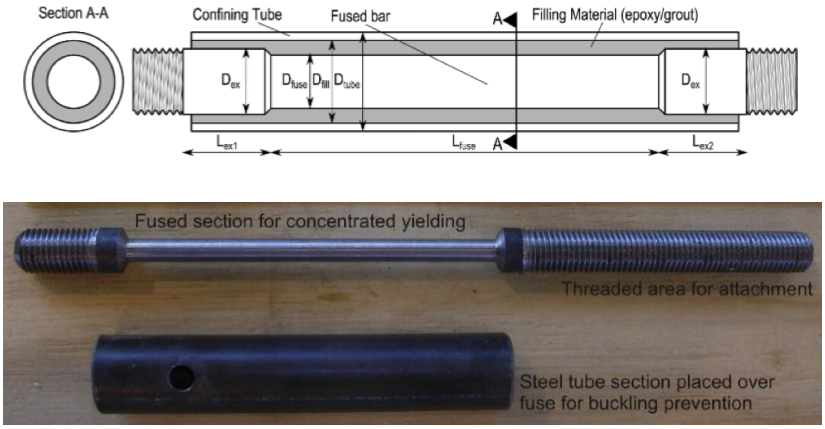

Figure 2. Schematic representation (Sarti et al., 2016) and real picture (modified after Smith, 2014) of the Plug&Play fuse-type external dissipater.

As previously mentioned, the simultaneous presence of re-centering capabilities provided by the post-tensioning cables, and the energy dissipation allowed by the yielding of the Plug&Play (or the internal mild steel bars) define the typical "flag-shaped" hysteresis rule of the PRESSS system (Figure 3). This hysteretic loop clearly demonstrates the near absence of residual displacements or deformations, which is further quantified by the re-centering ratio, λ, defined as the ratio between the contribution from the post-tensioning/axial load (i.e., re-centering action), and the one from the dissipaters (i.e., energy dissipation). The value of λ determines the degree of the flag shape, with higher values indicating increased self-centering capability. Generally, a λ value of 1.50, representing a 60-40 balance, generate a good level of energy dissipation while also guaranteeing the absence of residual displacement.

Funded by the European Union

This project has received funding from the European Union under the Horizon Europe Research & Innovation Programme (Grant Agreement no. 101123467 MultiCare). Views and opinions expressed are however those of author(s) only and do not necessarily reflect those of the European Union. Neither the European Union nor the granting authority can be held responsible for them.

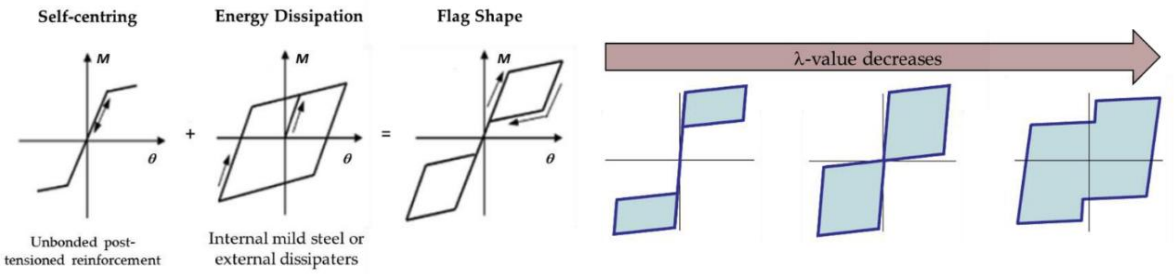

Figure 3. Flag-shaped hysteresis rule characterising the PRESSS technology (fib, 2003) and the effect of the re-centering ratio λ on the shape (NZCS, 2010).

2.2. The use of timber in post-tensioned structures: the Pres-Lam technology

Since the concept of post-tensioned rocking solutions is material-independent, the innovations developed through the PRESSS research program were subsequently extended to a variety of structural materials. These include steel (Christopoulos et al., 2002; Sause et al., 2006), timber - through the development of Pres-Lam technology - and hybrid solutions that combine these materials (Ruaumoko Solutions, 2012). In line with the main objectives of the MULTICARE Project, this technical handbook will focus on post-tensioned timber structures. By utilizing timber, the inherent sustainability of the material comes along the effective low-damage performance of the post-tensioned technology originally designed for precast concrete. The Prestressed Laminated timber technology, also known as Pres-Lam, was developed since 2005 at the University of Canterbury (Palermo et al., 2005; 2006; Pampanin et al., 2006). Developed primarily for Laminated Veneer Lumber (LVL), Pres-Lam structures can be made of both frames and walls (Figure 4a) using Glulam, CLT, or even Mass-Plywood Panels. This system avoids the need for many bolts or nails typical of the MRFs (i.e., Moment-Resisting Frames) connections, thanks to the use of post-tensioning. In line with the damage-control philosophy, the ductility of the system does not rely anymore on fasteners plasticization, which usually ends up to permanently damaging timber. Similarly to the PRESSS system, internal epoxied bars were also proposed for Pres-Lam (Figure 4b) (Palermo et al., 2005; 2006). However, by employing external Plug&Play dissipaters (Sarti et al., 2016), damage to the timber can be entirely avoided, provided that timber crushing parallel to the grain during rocking motion is prevented through proper section design.

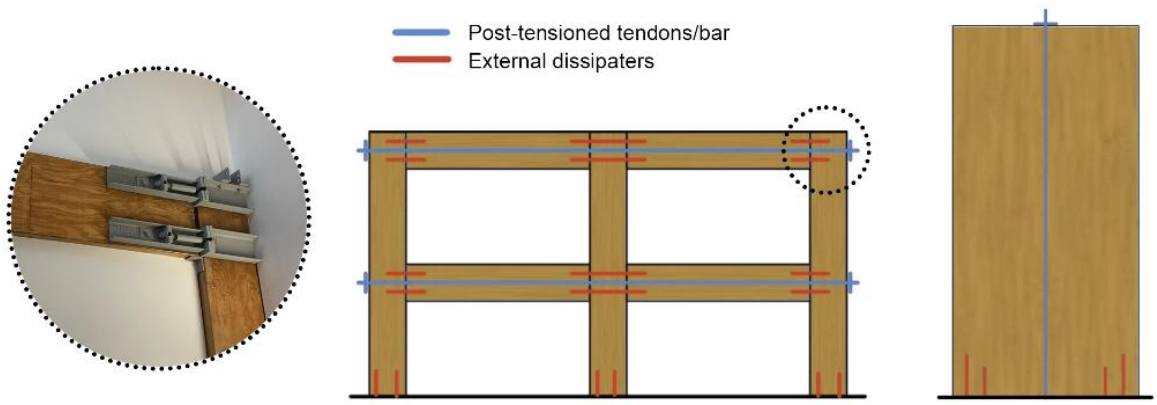

a)

This project has received funding from the European Union under the Horizon Europe Research & Innovation Programme (Grant Agreement no. 101123467 MultiCare). Views and opinions expressed are however those of author(s) only and do not necessarily reflect those of the European Union. Neither the European Union nor the granting authority can be held responsible for them.

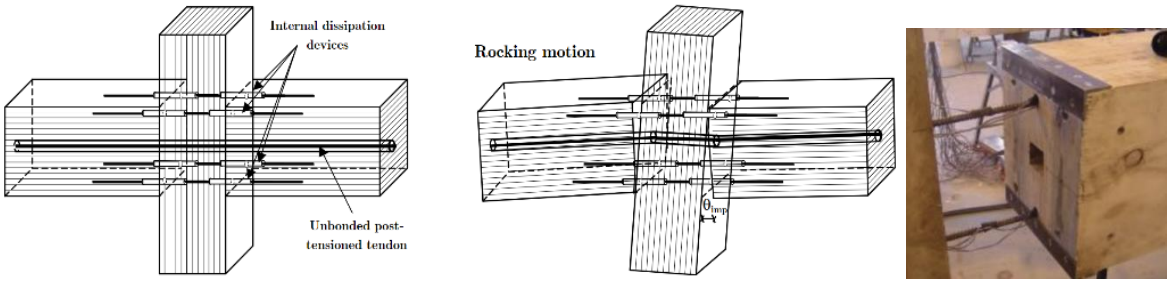

Figure 4. a) Schematic representation of Pres-Lam frames and walls with internal post-tensioned cables and external dissipaters (modified after Pampanin et al., 2013) and a detail of beam-column joint (photo taken by the author); b) Hybrid section with internal epoxied bars (Palermo et al., 2005).

Moreover, large open spaces are possible due to higher limits of span length that can be achieved, also using draped tendons (Palermo et al. 2010, van Beerschoten 2011). Pres-Lam buildings are characterized by architectural flexibility, in terms of both internal space and system modularity (Figure 5). This system can accommodate any building use, thanks to its high seismic performance and versatility/adaptability. The Pres-Lam technology has demonstrated its efficacy through extensive testing over the past two decades (Newcombe et al., 2010; Iqbal et al., 2010; Sarti et al., 2016; Moroder et al., 2018), and in real buildings when exposed to actual earthquakes (Smith et al., 2012; Holden et al., 2016; Granello et al., 2020).

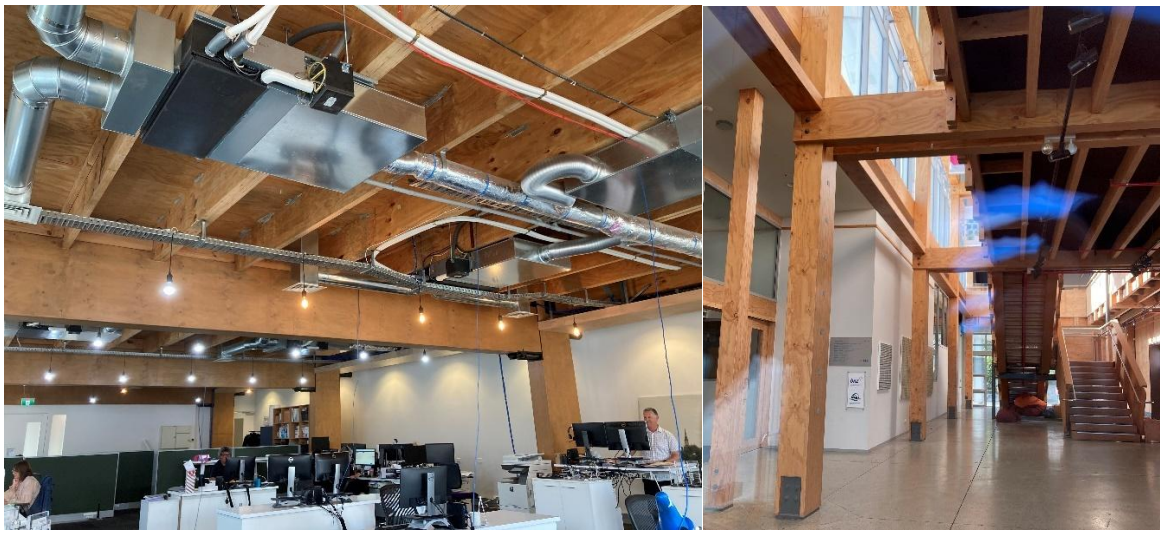

Figure 5. Examples of Pres-Lam large internal flexible spaces: the Young Hunter House building in Christchurch (New Zealand) on the left, hosting different building uses over the year; the Nelson Marlborough Institute of Technology (NMIT) building in Nelson (New Zealand) on the right, the first Pres-Lam building in the world, hosting public tertiary education activities (photos taken by the author). This last building displays draped tendons running within coupled beams, and post-tensioned coupled walls.

The key design parameters to describe the rocking dissipative mechanism in Pres-Lam hybrid connections is represented by the ratio β between the moment due to post-tensioning over the total moment, expressed by Equation 1:

$$\beta = \frac{M_{pt}}{M_s + M_{pt}} \quad (1)$$

Funded by the European Union

This project has received funding from the European Union under the Horizon Europe Research & Innovation Programme (Grant Agreement no. 101123467 MultiCare). Views and opinions expressed are however those of author(s) only and do not necessarily reflect those of the European Union. Neither the European Union nor the granting authority can be held responsible for them.

Where M_{pt} represents the re-centering moment contribution, and M_s the energy dissipation contribution. In order to guarantee a fully re-centering of the connections, a value of $\beta>0.5$ should be used, corresponding to the λ value of 1.5 already mentioned. Although designer might opt for a post-tensioning only solution (i.e., a value of β equal to 1) for low seismic regions, it is still recommended to provide energy dissipation devices by therefore employing hybrid connections (Granello et al., 2020). Dissipaters, in fact, can provide capacity to the system even after the post-tensioned tendons (remote) failure, and they also help to prevent post-tensioning losses (Granello et al., 2017).
The design of Pres-Lam connections is conceptually identical to the design of post-tensioned concrete (i.e., PRESSS) structures (Pampanin, 2010). The steps for designing such low-damage timber structures will be explained in the following paragraphs. The main significant difference between seismic design of post-tensioned precast RC buildings and timber buildings lies in the elastic deformation of the latter. Apart from the reduced Modulus of Elasticity – which is compensated by reduced weight, resulting in nearly the same member size – timber buildings experience larger elastic deformation under earthquake actions, causing the gap opening at the rocking interface to occur later.

2.3. Pres-Lam structures for the rehabilitation of existing buildings

Although the Pres-Lam can be considered as a promising technology to support the design of seismic resilient new buildings, it should be stressed that almost 80% (Gkatzogias et al., 2022) of buildings in Europe have been erected disregarding modern seismic regulations. As a result, most of the existing building stock is vulnerable to seismic loading, as confirmed by recent devastating earthquakes which affected several regions around the world (e.g., L'Aquila 2009, Italy; Canterbury Region 2010-2011, New Zealand; Central Italy, 2016-2017; and Turkey and Syria, 2023).
Such a vulnerability is linked to past design practices related only to gravity loads. Indeed, buildings constructed before the enforcement of modern seismic codes were designed by following an elastic approach based on "working stresses", thus disregarding the concepts of "capacity design" and "hierarchy of strength" (Park & Pauley, 1975). For these reasons, existing buildings are not capable of accommodating inelastic demand related to earthquake loading, potentially resulting in brittle failures (e.g., shear failures of structural components), leading to global collapse (Pampanin, 2006; De Luca et al., 2018).
In this perspective, the adoption of external low-damage exoskeletons designed following Displacement-Based Retrofit (DBR) procedures represents a remarkable opportunity to enhance the seismic resilience of the existing building stock. Indeed, the exoskeleton works as an additional structural system in parallel to the existing structure.
Moreover, the exoskeleton can support a high multi-performance double-skin facade system, also supporting energy refurbishment and architectural renovation, thus potentially fostering holistic renovation of the built environment, Figure 6. Further information related to the holistic renovation of buildings using such an exoskeleton solution can be found in Deliverable 13.3 "*End-user oriented guidelines for holistic retrofit*".

Funded by the European Union

This project has received funding from the European Union under the Horizon Europe Research & Innovation Programme (Grant Agreement no. 101123467 MultiCare). Views and opinions expressed are however those of author(s) only and do not necessarily reflect those of the European Union. Neither the European Union nor the granting authority can be held responsible for them.

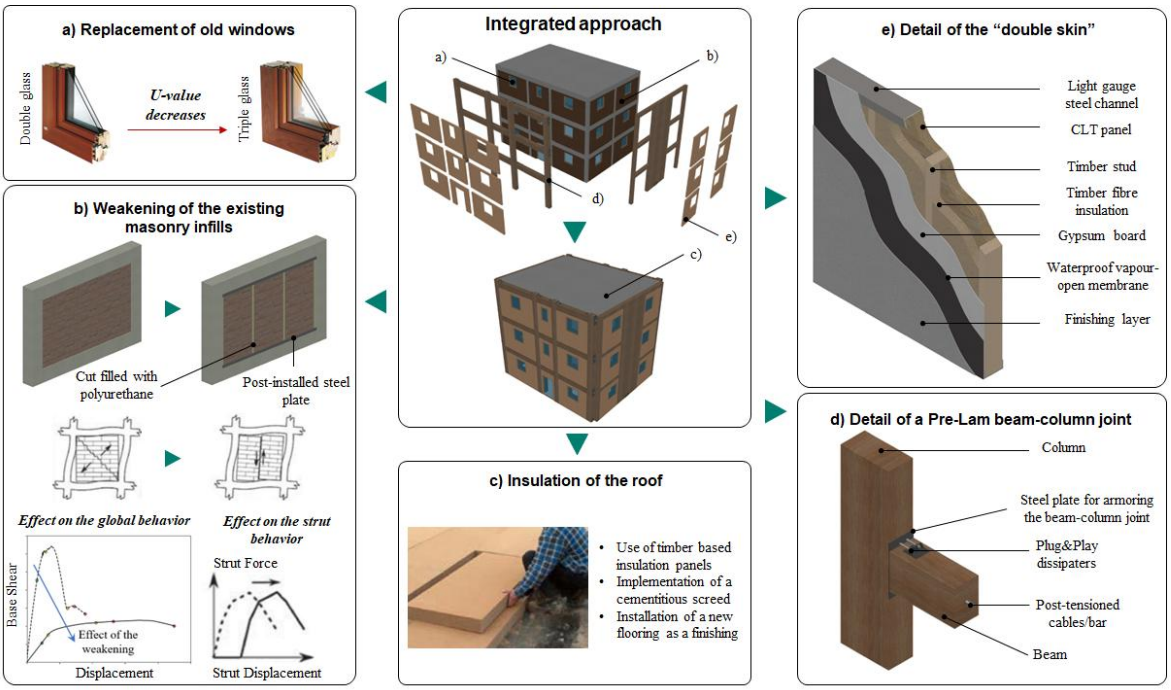

Figure 6. Schematic representation of the integrated intervention proposed, consisting of: a) replacing old windows, b) selective weakening of the existing masonry infills, c) roof insulation, d) use of Pres-Lam technology for the external exoskeleton, illustrated for a beam-column joint, and e) implementation of a low-damage timber based "double-skin" façade system for the insulation of the vertical building envelope.

3. Seismic design of Pres-Lam structures and Exoskeleton Systems

3.1. Direct Displacement-Based Design (DDBD)

To date, the Direct Displacement-Based Design (DDBD) procedure has become a powerful alternative approach to current force-based design procedures, representing a significant shift in the seismic design philosophy due to the recognition of the primary role of displacements as reliable and direct indexes of structural (and non-structural) damage. This approach has been developed by Priestley, 2002, Priestley et al., 2007 as a simple method of designing a structure to achieve a set of target displacement limits by characterizing the structure's effective stiffness (secant to the target displacement) - instead of initial stiffness as estimated in force-based procedures - and a level of equivalent elastic damping, which combines the effects of elastic and hysteretic damping. This method therefore does not require the estimation of the structure's initial period; however, it does require the assumption of the structure's displaced shape at yield and of the design deflection envelope.

The general procedure for DDBD is shown in Figure 7. Through this methodology, the structure is converted into a single-degree-of-freedom (SDOF). By imposing a design drift, the effective (secant) period of the SDOF system can be evaluated from the displacement spectra, which is reduced by the R factor as a function of the structural damping. In this way, the structure is characterized by an effective stiffness depending on the target design drift and on the structural damping, which is a combination of elastic and hysteretic damping.

Funded by the European Union

This project has received funding from the European Union under the Horizon Europe Research & Innovation Programme (Grant Agreement no. 101123467 MultiCare). Views and opinions expressed are however those of author(s) only and do not necessarily reflect those of the European Union. Neither the European Union nor the granting authority can be held responsible for them.

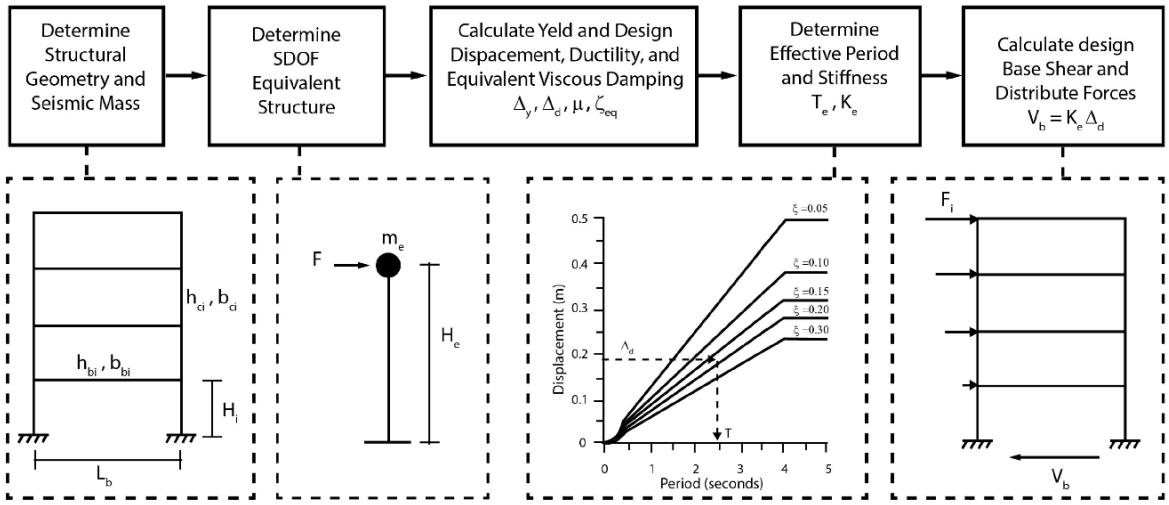

Figure 7. The Direct Displacement-Based Design methodology (modified after Priestley et al., 2007).

To account for the use of timber in the post-tensioned structural system, some adjustments must be made in the design procedure. Indeed, the higher elastic deformability of the components before the rocking motion activation should be considered in the case of the Pres-Lam technology. For this technology, the Serviceability Limit State (SLS) generally governs the size of the components and the amount of post-tensioning. Consequently, the structural members are dimensioned to carry the force-demand at the SLS, and then designed in detail and verified at the Ultimate Limit State (ULS) (Miliziano, 2019; Pampanin et al., 2013) as illustrated in Figure 8. A step-by-step design of a case-study application will be presented in the next paragraphs, specifically focusing on the use of Pres-Lam technology for the rehabilitation of existing buildings.

Funded by the European Union

This project has received funding from the European Union under the Horizon Europe Research & Innovation Programme (Grant Agreement no. 101123467 MultiCare). Views and opinions expressed are however those of author(s) only and do not necessarily reflect those of the European Union. Neither the European Union nor the granting authority can be held responsible for them.

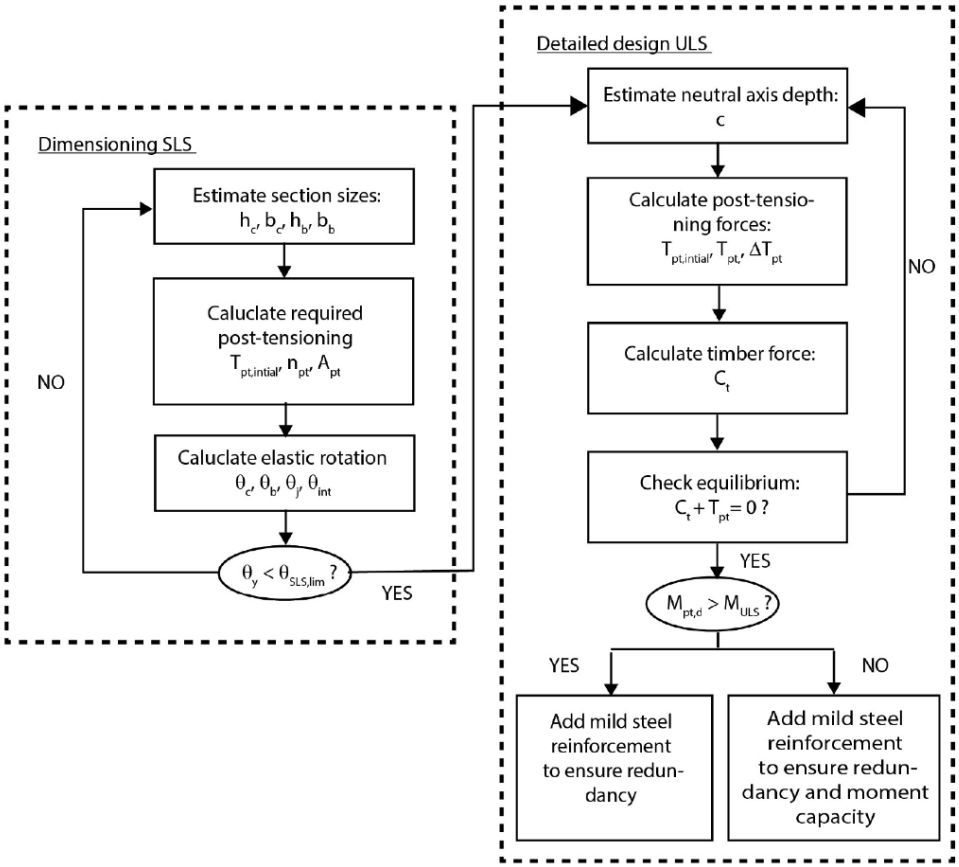

Figure 8. Flow chart of the modified Displacement-Based Design procedure for post-tensioned timber structures (modified after Miliziano, 2019).

3.2. Displacement-Based Retrofit (DBR)

The Displacement-Based Retrofit (DBR) procedure presented herein can be considered as an extension of the DDBD procedure to design new buildings (§3.1). The main goal of the DBR procedure, which supports the design of the exoskeleton, is to prevent the existing structure from reaching and exceeding the failure displacement profile. Such a failure displacement profile is defined by means of the seismic assessment of the considered existing structure. Such a maximum displacement that the existing structure can withstand can be adopted as a target in the procedure itself.

Clearly, based on cost-benefit considerations, further reduced values can be adopted to enhance the performance of the retrofitted structure. In any case, while on one hand selecting reduced displacement can enhance performance, since the maximum experienced displacement is well recognised as a damage indicator, on the other, reducing the maximum displacement increases accelerations and forces the retrofitted structure must withstand. This aspect can present challenges both for the connection systems between the existing structure and the exoskeleton (§5.2.3), as well as for the capacity of the existing building's slabs.

In this document, the DBR procedure for supporting the design of exoskeletons based on the Pres-Lam technology is presented in detail. It is worth noting that in the case of the Pres-Lam technology (i.e., timber components), minor adjustments should be made in respect to the concrete-based counterpart (e.g., when PRESSS technology is adopted, D'Amore & Pampanin, 2025). Indeed, when dealing with timber components, their higher deformability before the activation of the rocking mechanism (especially related to beam-

Funded by the European Union

This project has received funding from the European Union under the Horizon Europe Research & Innovation Programme (Grant Agreement no. 101123467 MultiCare). Views and opinions expressed are however those of author(s) only and do not necessarily reflect those of the European Union. Neither the European Union nor the granting authority can be held responsible for them.

column joints) should be properly addressed. Specifically, when dealing with concrete structures, the DDBD or DBR procedures allow the definition of the detailed design of the components and connection systems at the Life-Safety Limit-State (LSLS), and subsequently, the Damage-Control Limit-State (DCLS) is checked. In the case of timber structures, the DCLS generally governs the size of structural components and the amount of post-tensioning. This is crucial to prevent damage to both the as-built structure and non-structural components in the case of frequent earthquakes. After calculations at the DCLS have been carried out, it is possible to finalise the design at the LSLS, thus providing the correct amount of external Plug&Play dissipaters to meet the seismic demand at the LSLS. In other words, when dealing with Pres-Lam technology, two design steps should be considered, as illustrated in Figure 9.

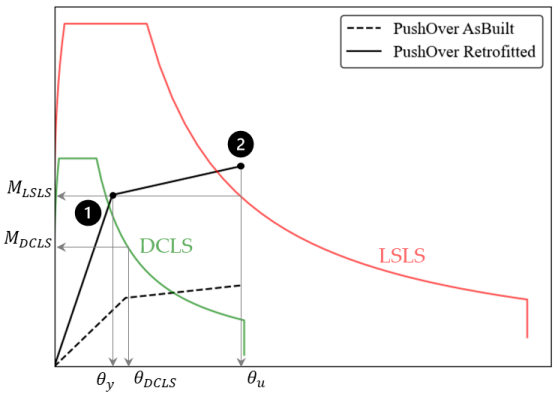

❶ Equivalent yielding point.
Design requirements ➔ $\theta_y \leq \theta_{DCLS}$
$M_y \geq M_{DCLS}$

❷ Ultimate point
Design requirements ➔ $M_u \geq M_{DCLS}$

Figure 9. Design process for timber-based exoskeletons.

- ***Step 1***: Section sizes and amount of post-tensioning must be defined to ensure that the elastic deformation of the frame, θ_y, is less than the imposed limit drift for the DCLS, θ_{DCLS}. Such a value can be defined based on the assessment of the as-built structure and in accordance with national building codes. For example, according to the Italian Building Code, NTC (2018), θ_{DCLS} is defined as the minimum between the drift causing the achievement of the equivalent yielding point of the as-built structure and the one inducing damage to non-structural components (i.e., 0.50%). Clearly, in this step, it should also be verified that all the connections remain elastic (i.e., $M_y \geq M_{DCLS}$). Major information related to the DBR procedure for the DCLS is provided in the following paragraph §3.2.1.

- ***Step 2***: Once the verification for the DCLS has been carried out, the DBR procedure at the LSLS can be implemented. After defining the internal actions, it is possible to implement a detailed connection design for the LSLS and carry out the final verifications (i.e., $M_u \geq M_{LSLS}$).

3.2.1 The Displacement-Based Retrofit Procedure for the Damage-Control Limit-State

As mentioned before, when dealing with timber-based exoskeletons, the size of components and the amount of post-tensioning should be defined to ensure that the elastic deformation of the exoskeleton itself (i.e., θ_y) is less than the limit drift imposed at the DCLS (i.e., θ_{DCLS}).
The total elastic deformation of the frame can be defined from Equation 2.

$$\theta_y = \frac{\sum_{i=1}^{N} M_{con\,i,DCLS}\theta_{y,i}}{\sum_{i=1}^{N} M_{con\,i,DCLS}} \quad (2)$$

This project has received funding from the European Union under the Horizon Europe Research & Innovation Programme (Grant Agreement no. 101123467 MultiCare). Views and opinions expressed are however those of author(s) only and do not necessarily reflect those of the European Union. Neither the European Union nor the granting authority can be held responsible for them.

In this equation, $M_{con\,i,DCLS}$ stands for the capacity of the connection, at the i-th storey and at the DCLS. $\theta_{y,i}$ is the elastic connection rotation at the i-th storey, while N is the number of storeys.
In order to define $M_{con\,i,DCLS}$, the first step requires the implementation of the DBR procedure to define the base shear corresponding to the DCLS. In this specific case, the design drift to be used as an input for the DBR, θ_{DCLS}, is defined as the minimum between the one causing the attainment of the equivalent yielding point of the as-built structure, and the one defined to prevent damage in non-structural components (i.e., 0.50% according to NTC 2018 for masonry infills, largely adopted as an envelope for RC constructions). When applying the DBR for the DCLS, the definition of the equivalent viscous damping is not required since the elastic 5%-damped displacement spectra at DCLS must be used. Once the base shear corresponding to the considered LS is defined, it is possible to implement an equilibrium approach for defining the capacity moment in each connection.
The capacity moment to be provided (i.e., $M_{con\,i,DCLS}$) allows to define the amount of post-tension to ensure that the connection remains elastic. More specifically, according to Priestley & Tao (1993), the behaviour of a post-tensioned connection can be represented with a non-linear moment-rotation curve in which two points can be identified, Figure 10:

- ***Point 1***: Decompression point at which compression in the extreme fibre is lost;
- ***Point 2***: The point where the centroid of the connection reaches decompression. According to Priestley & Tao (1993), such a point is achieved when the acting moment is about two times the decompression one.

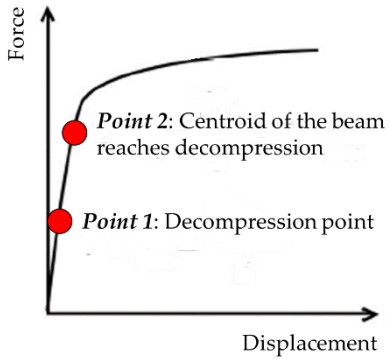

Figure 10. Behaviour of a post-tensioned connection in terms of force-displacement relationship (modified after Priestley & Tao, 1993).

Considering the definition given for the point 2, it is possible to impose Equation 3 to ensure that the yielding point is not reached at the DCLS.

$$2M_{Dec} \simeq M_{con\,i,DCLS} \tag{3}$$

The decompression moment is instead defined in Equation 4.

$$M_{Dec} = \frac{T_{pt,initial}\,h_b}{3} \tag{4}$$

In Equation 4, $T_{pt,initial}$ is the amount of initial post-tensioning to be provided. Finally, by substituting Equation 4 in Equation 3, it is possible to define the amount of initial post-tension to ensure that the connection remains elastic for the demand imposed at the DCLS, Equation 5.

$$T_{pt,initial} = \frac{3M_{con\,i,DCLS}}{h_b} \tag{5}$$

This project has received funding from the European Union under the Horizon Europe Research & Innovation Programme (Grant Agreement no. 101123467 MultiCare). Views and opinions expressed are however those of author(s) only and do not necessarily reflect those of the European Union. Neither the European Union nor the granting authority can be held responsible for them.

After the definition of the amount of post-tensioning it is also possible defining the elastic deformation of the connections, $\theta_{y,i}$. Such an elastic deformation can be defined based on the elastic deformation of all the components framing in the connection itself (Smith *et al.* 2014), as illustrated in Figure 11. Such contributions are: i) the elastic beam deformation, θ_b (Equation 6); ii) the elastic column deformation, θ_c (Equation 7a and 7b, for interior and exterior columns, respectively); iii) the elastic joint deformation, θ_j (Equation 8a and 8b, for interior and exterior joints, respectively); and iv) the connection deformation, θ_{con}, which depends on two contributions. Such two contributions are the interface compression deformation, θ_{int} (Equation 9) initially proposed by Van Beerschoten *et al.* (2011), and the gap deformation, θ_{gap}. It is worth noticing that when dealing with the calculation at the DCLS, $\theta_{gap} = 0$ since the rocking motion is not activated.

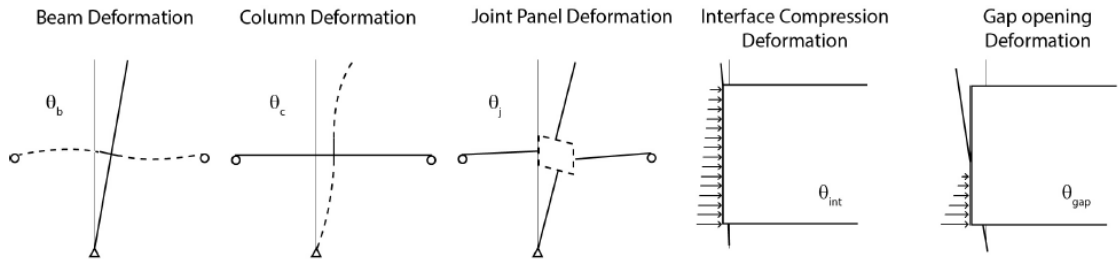

Figure 11. Rotation contributions to post-tensioned timber frames (Smith et al. 2014).

$$\theta_b = \frac{M_{con\,i,DCLS}}{L_b}\left(\frac{(L_b - h_c)^2}{6E_t I_b} + \frac{2\alpha_{s,cl}}{G_t A_b}\right) \tag{6}$$

$$\theta_{c,Int} = \frac{M_{con\,i,DCLS}}{(L_b - h_c)}\left(\frac{H_C}{6E_t I_c} + \frac{2\alpha_{s,cl}}{G_t A_c H_C}\right) \tag{7a}$$

$$\theta_{c,Ext} = \frac{1}{2}\frac{M_{con\,i,DCLS}}{(L_b - h_c)}\left(\frac{H_C}{6E_t I_c} + \frac{2\alpha_{s,cl}}{G_t A_c H_C}\right) \tag{7b}$$

$$\theta_{j,Int} = (2 - \beta)\frac{3M_{con\,i,DCLS}}{2\alpha_{s,ave} A_c h_b G_t} \tag{8a}$$

$$\theta_{j,Ext} = \frac{3M_{con\,i,DCLS}}{2\alpha_{s,ave} A_c h_b G_t} \tag{8b}$$

$$\theta_{int} = k_{int}\frac{T_{pt,initial} h_c}{E_{t\perp} h_b^2 b_b} \tag{9}$$

In the equations above h_c and H_c stand for the column depth and height, respectively. b_b is the width of the beam. I_b and I_c are the second moment of area of the beam and of the column, respectively, while A_b is the cross-sectional area of the beam and A_c the cross-sectional area of the column. E_t and $E_{t\perp}$ are the modulus of elasticity parallel and perpendicular to the grain, respectively, while G_t is the shear modulus of timber. $\alpha_{s,cl}$ is the shear coefficient to convert the average shear to the centroidal shear and can be assumed as 3/2 for rectangular sections. $\alpha_{s,ave}$ is the effective shear area factor and is assumed equal to 0.85.

Finally, k_{int} is the interface compression factor accounting for load sharing and considers the typology of interface reinforcement (Smith *et al.* 2014). More specifically, $k_{int} = 0.85$ in case of no reinforcement at the interface. Such configurations should be strongly discouraged, especially in the case of deep beam-shallow column, Figure 12a. The k_{int} values can be reduced in case of reinforcement of the joint. More specifically, k_{int} is within the range 0.4-0.6 in the case of screw-based reinforcement, Figure 12b. In this case, screws

Funded by the European Union

This project has received funding from the European Union under the Horizon Europe Research & Innovation Programme (Grant Agreement no. 101123467 MultiCare). Views and opinions expressed are however those of author(s) only and do not necessarily reflect those of the European Union. Neither the European Union nor the granting authority can be held responsible for them.

act similarly to piled foundations, allowing for better diffusing compressive forces. Finally in the case of steel-based reinforcement, Figure 12c, k_{int} is equal to 0.2. This is the best solution as the implementation of steel plates and steel rods allows bypassing the beam-column joint itself.

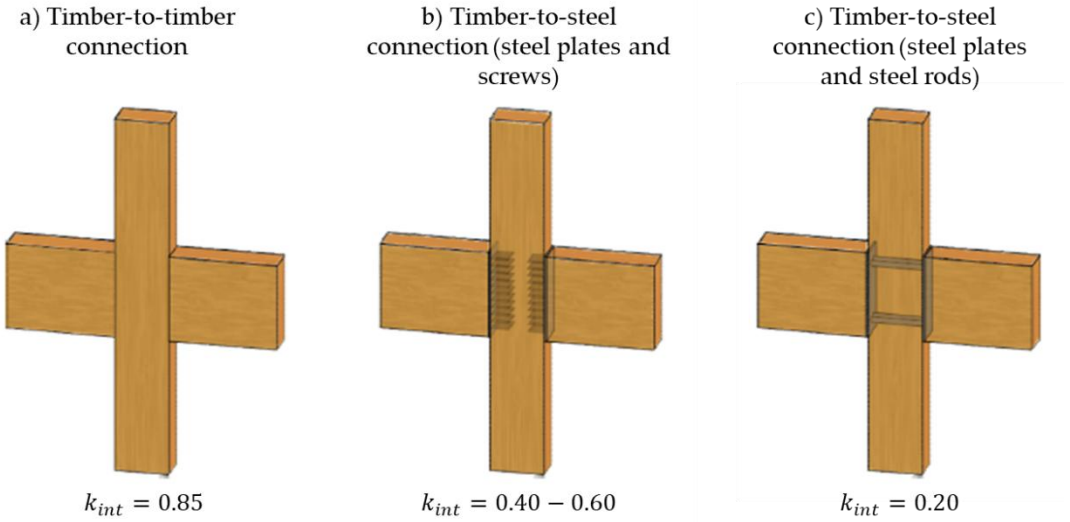

Figure 12. k_{int} values for alternative reinforcements of the beam-column joint. a) timber-to-timber connection, b) timber-to-steel connection using steel plates and screws, and c) timber-to-steel connection implementing steel plates and steel rods. Modified after Smith et al., 2014.

Once all the contributions have been defined, it is possible to define the elastic deformation of the connection by using Equation 10.

$$\theta_{y,i} = \theta_{b,i} + \theta_{c,i} + \theta_{j,i} + \left(1 - \frac{h_c}{L_b}\right)\theta_{int,i} \quad (10)$$

Where $\left(1 - \frac{h_c}{L_b}\right)$ allows to translate the interface rotation from the column interface to the centreline. Using $\theta_{y,i}$, it is possible to define the total elastic deformation of the frame, by using Equation 2, and verify that such a value is minor than the design drift used at the beginning of the procedure (i.e., $\theta_y \leq \theta_{D,DCLS}$).
Additionally, it is worth stressing that along with the higher elastic deformations when compared to other materials, timber is also characterised by an anisotropic nature, with significantly lower stiffness in the perpendicular-to-the-grain direction. This means that where timber parallel to the grain is bearing on timber perpendicular to the grain, interaction between the two surfaces reduces the overall stiffness of the connection. To this end, the connection modulus of elasticity is equal to the modulus of elasticity parallel to the grain multiplied by a reduction gap, k_{gap}, which accounts for the joint reinforcement perpendicular to the grain, as illustrated in Table 3.

Funded by the European Union

This project has received funding from the European Union under the Horizon Europe Research & Innovation Programme (Grant Agreement no. 101123467 MultiCare). Views and opinions expressed are however those of author(s) only and do not necessarily reflect those of the European Union. Neither the European Union nor the granting authority can be held responsible for them.

Table 3. k_{gap} values for post-tensioned timber buildings (Pampanin et al., 2013)

	Occurrence	k_{gap}
Situations where no perpendicular to the grain action is present.	Wall-to-foundation, column-to-foundation connections, beam-column connections with concrete columns.	0.70
Situations where perpendicular to grain action is present but adequate measures have been made to protect the perpendicular to grain crushing of timber.	Beam-column joints reinforced with screws, epoxied in rods, etc.	0.55
Situations where perpendicular to grain action is present and no effort has been made to protect perp to grain crushing of timber.	Unreinforced beam-column joints (not recommended)	0.10

Finally, after verifying the DCLS, the DBR procedure can be implemented at the LSLS to finalise the design. The elastic deformation θ_y, previously calculated, can be used together with the design drift $\theta_{u,LSLS}$ to define the ductility μ of the system. Consequently, the equivalent viscous damping related to the exoskeleton can be evaluated. After defining the internal actions at the LSLS, it is possible to implement a detailed connection design for such an LS and carry out the final verifications (i.e., $M_u \geq M_{LSLS}$). In this step, the dissipaters must be added to the amount of post-tensioning previously designed to ensure the desired moment capacity. In case the calculations for the LSLS do not require additional reinforcement with respect to the one provided at the DCLS, additional dissipaters are considered to ensure redundancy. The DBR procedure at the LSLS is detailed in the following paragraph § 3.2.2.

3.2.2. The Displacement-Based Procedure at the Life-Safety Limit-State

In this paragraph, the DBR procedure at the LSLS will be presented. The procedure is schematically illustrated in Figure 13.

Funded by the European Union

This project has received funding from the European Union under the Horizon Europe Research & Innovation Programme (Grant Agreement no. 101123467 MultiCare). Views and opinions expressed are however those of author(s) only and do not necessarily reflect those of the European Union. Neither the European Union nor the granting authority can be held responsible for them.

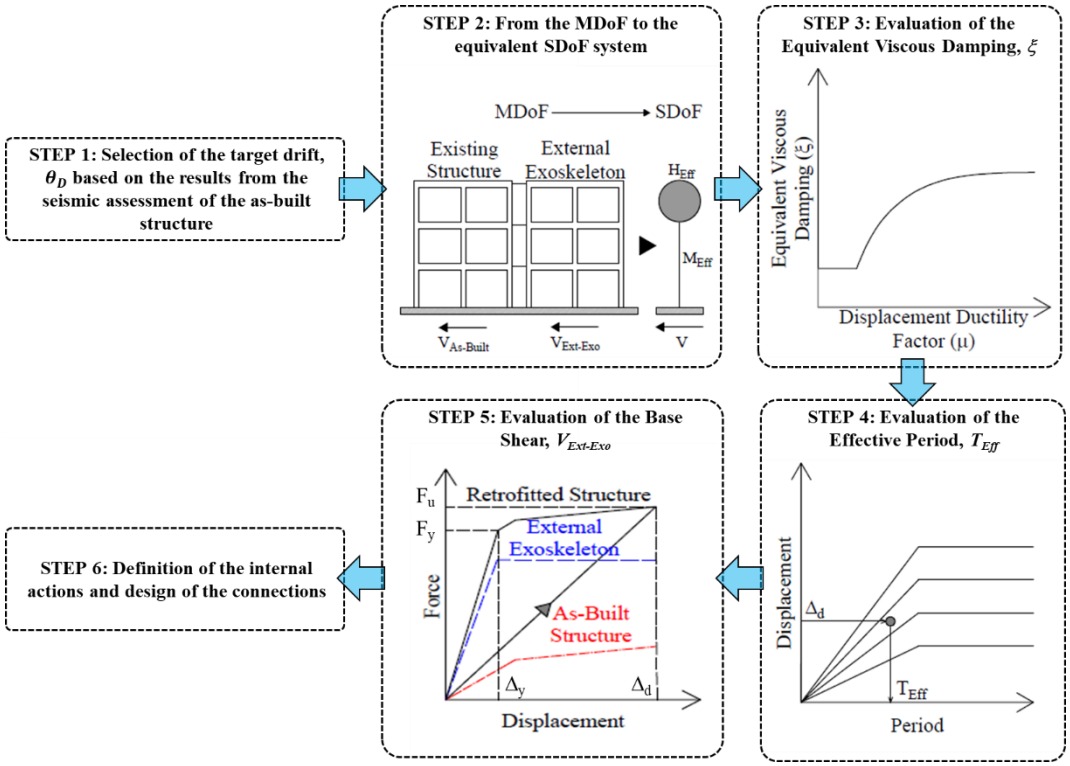

Figure 13. Flow-chart of the steps of the Displacement-Based Retrofit (DBR) procedure.

The main steps of the procedure are discussed in detail in the following:

- ***Step 1***: Selection of the target drift θ_D. Specifically, in this case, the maximum allowable displacement for the as-built structure has been used as a target (i.e., $\theta_{u,LSLS}$). By converting the seismic response of the as-built Multi-Degree of Freedom System (MDoF) into a Single Degree of Freedom (SDoF) within the Acceleration-Displacement Response Spectrum (ADRS) domain, it is possible to define θ_D from Equation 11:

$$\theta_D = \frac{\Delta_{Max,AB}}{H_{Eff,AB}} \quad (11)$$

  Where $\Delta_{Max,AB}$ and $H_{Eff,AB}$ are the maximum allowable displacement and the effective height of the equivalent SDoF system representative of the as-built structure. In any case, when the failure mechanism of the structure is governed by the crisis of external beam-column joints, as expected for existing and poorly detailed buildings, the design drift can be set equal to 1.00%, as suggested by Pampanin *et al*., 2003.

- ***Step 2***: The MDoF retrofitted structure is converted into an equivalent SDoF system, and the relevant parameters (i.e., the design displacement Δ_d, the effective mass m_{Eff}, and the effective height H_{Eff} are defined using the formulations proposed in Priestley (2002), and reported in Equations 12, 13, and 14. All these quantities are functions of the story mass m_i, the story design displacement Δ_i, and the story height h_i, whereas N is the total number of stories.

$$\Delta_D = \frac{\sum_{i=1}^{N}(m_i\Delta_i)^2}{(m_i\Delta_i)} \quad (12)$$

This project has received funding from the European Union under the Horizon Europe Research & Innovation Programme (Grant Agreement no. 101123467 MultiCare). Views and opinions expressed are however those of author(s) only and do not necessarily reflect those of the European Union. Neither the European Union nor the granting authority can be held responsible for them.

$$m_{Eff} = \frac{\sum_{i=1}^{N}(m_i \Delta_i)}{\Delta_d} \quad (13)$$

$$H_{Eff} = \frac{\sum_{i=1}^{N}(m_i \Delta_i h_i)}{(m_i \Delta_i)} \quad (14)$$

- ***Step 3***: The equivalent viscous damping ξ of the system is defined through Equation 15. Specifically, such a value is defined by weighting in proportion to the base shear carried by the as-built structure and by the exoskeleton, respectively. The equivalent viscous damping for the as-built structure has been derived following the recommendations reported in NTC (2018), Equation 16. Concerning the Pres-Lam exoskeleton, the formulation available in Pampanin *et al.* (2013) has been adopted, Equation 17.

$$\xi = \frac{\xi_{AB} V_{B,AB} + \xi_{Exo} V_{B,Exo}}{V_{B,AB} + V_{B,Exo}} \quad (15)$$

$$\xi_{AB} = k \frac{63.7\left(a_y^* d_{max}^* - a_{max}^* d_y^*\right)}{a_{max}^* d_{max}^*} + 5 \quad (16)$$

$$\xi_{Exo} = 5\% \cdot \mu^{-0.43} + 0.65 \cdot \frac{(2-2\beta)(\mu-1)}{\mu\pi\left(1 + r(\mu-1)\right)} \quad (17)$$

In Equation 15, ξ_{AB} and ξ_{Exo} represent the equivalent viscous damping of the as-built structure and of the exoskeleton, respectively. $V_{B,AB}$ denotes the base shear carried by the as-built structure, while $V_{B,Exo}$ the one carried by the exoskeleton. In Equations 16, μ stands for the ductility (also in Equation 17), a_y and d_y represent the acceleration and displacement, respectively, defined through the equivalent yielding point identified by the bilinear curve of the as-built structure in the Acceleration-Displacement Response Spectrum (ADRS) format. On the other hand, a_{max} and d_{max} represent the acceleration and displacement achieved at the attainment of the LSLS. The k factor is herein set equal to 0.33. Such a value is adopted for considering the low energy dissipation capabilities of existing, poorly detailed buildings. In Equation 17, λ is the recentring ratio adopted, r is the post-yield stiffness ratio, and β is defined as the ratio between the re-centring contribution (i.e., M_{PT}) and the total moment of the connection (i.e., M_{Tot}). Clearly, considering the definition of β, it is easy to understand that such a coefficient is strictly related to the re-centring ratio (i.e., $\beta = \lambda/(\lambda+1)$).
It is worth mentioning that the formulations for deriving the equivalent viscous damping are strictly dependent on the ductility μ of the system, defined as the ratio between the design displacement and the yielding one. Specifically, when dealing with the as-built structure, the ductility can be derived from the assessment procedure, whilst in the case of the exoskeleton, which must be designed, the formulation presented in Equation 2 should be adopted.

- ***Step 4***: The effective period T_{Eff} is derived from the damped displacement spectrum, at the Life Safety Limit State (LSLS), using the design displacement Δ_d defined in ***Step 2*** (Equation 12). The ξ factor reported in Equation 15, and depending on the equivalent viscous damping defined in ***Step 3***, is used to define the damped spectrum:

$$R_\xi = \sqrt{\frac{10}{5+\xi}} \quad (18)$$

- ***Step 5***: The effective stiffness K_{Eff} is derived from the effective period T_{Eff} through Equation 19. Using $K_{Eff,}$ it is possible to define the base shear carried by the

This project has received funding from the European Union under the Horizon Europe Research & Innovation Programme (Grant Agreement no. 101123467 MultiCare). Views and opinions expressed are however those of author(s) only and do not necessarily reflect those of the European Union. Neither the European Union nor the granting authority can be held responsible for them.

retrofitted structure V_B, and knowing the one carried by the as-built structure, it is possible to define the base shear carried by the exoskeleton itself, Equation 20.

$$K_{Eff} = m_{Eff}\left(\frac{2\pi}{T_{Eff}}\right)^2 \quad (19)$$

$$V_{B,Exo} = V_{B,Tot} - V_{B,AB} = K_{Eff}\Delta_d - V_{B,AB} \quad (20)$$

- ***Step 6***: The base shear defined in ***Step 5*** is then distributed along the height of the exoskeleton following an equilibrium approach, and the internal actions are derived and used to detail all the beam-to-column and column-to-foundation connections.

4. Case-Study Application

This chapter illustrates an application for the design of a Pres-Lam exoskeleton for the seismic retrofit of an existing RC structure. After the presentation of the case study building, the results of the seismic assessment in the as-built configuration will be presented. After this, the DBR procedure will be implemented, and the exoskeleton will be designed according to the results of the analytical procedure.

4.1. Selected case study building.

The case study building considered in this application is an archetype building derived from the information available from the "Bonefro Building" (Figure 14), an Italian building quite "famous" in the scientific literature, which was severely damaged by the "San Giuliano di Puglia Earthquake" in 2002 (Decanini et al., 2004). Both the acceleration and displacement spectra for Bonefro at the Life-Safety Limit-State (LSLS, probability of occurrence equal to 10% in 50 years, Return Period equal to 475 years) are shown in Figure 15. The present case study is for residential use and is located in Bonefro. The case study is a four-story RC-infilled frame building with a plan of 19.50 m x 10.05 m, and an inter-story height equal to 3.10 m. Concerning the structural system, the building presents three Moment-Resisting Frames (MRFs) in the longitudinal direction (the two perimetral frames have deep beams, while the central one features hidden beams), and four MRFs in the transversal one (two perimetral frames with deep beams, while the others have hidden beams).

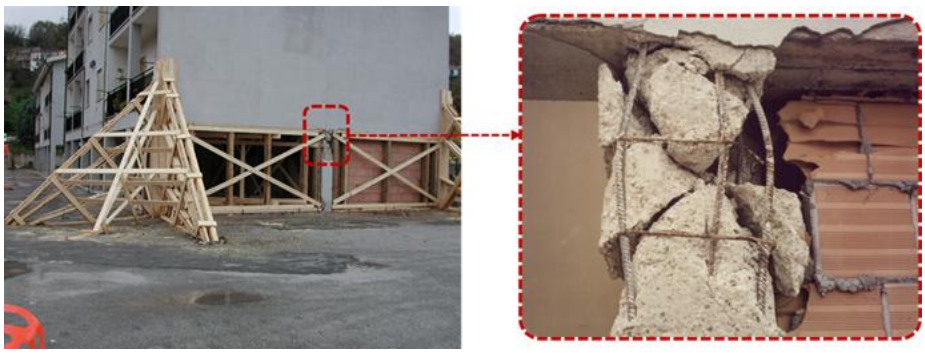

Figure 14. Bonefro building damaged during the San Giuliano di Puglia Earthquake (left), with identification of a brittle shear failure in the RC column due to interaction between the RC frame and the masonry infills, modified after Decanini et al., 2004.

Funded by the European Union

This project has received funding from the European Union under the Horizon Europe Research & Innovation Programme (Grant Agreement no. 101123467 MultiCare). Views and opinions expressed are however those of author(s) only and do not necessarily reflect those of the European Union. Neither the European Union nor the granting authority can be held responsible for them.

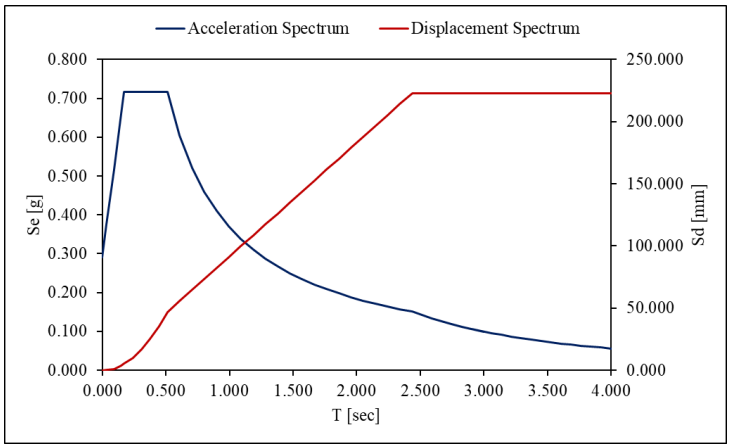

Figure 15. Acceleration and Displacement Spectra for Bonefro at the LSLS.

The building has been designed for gravity loads only and by following a "working stress" approach, thus lacking any considerations related to "capacity design" and "hierarchy of strengths" as imposed by modern seismic codes. Consequently, the building is expected to reflect the typical deficiencies/vulnerabilities of buildings erected in the pre-code era, and thus it is expected to be "potentially" seismic-prone.
Figure 16 illustrates the geometric characteristics of the considered building in terms of plan view.
Concerning the mechanical properties of materials, concrete has a compressive strength equal to 20 MPa, with a peak (ε'_c) and ultimate strain (ε_{cu}) equal to 0.0020 and 0.0035, respectively. Concerning reinforcing steel, in line with the properties of deformed bars realized using FeB44k, the yielding (f'_y) and ultimate (f'_u) stress have been considered equal to 430 MPa and 540 MPa, respectively, while the ultimate strain (ε_{su}) has been set equal to 0.004 in line with the prescriptions of the Italian Building Code (NTC 2018). The mechanical characteristics of materials are summarised in Table 4.

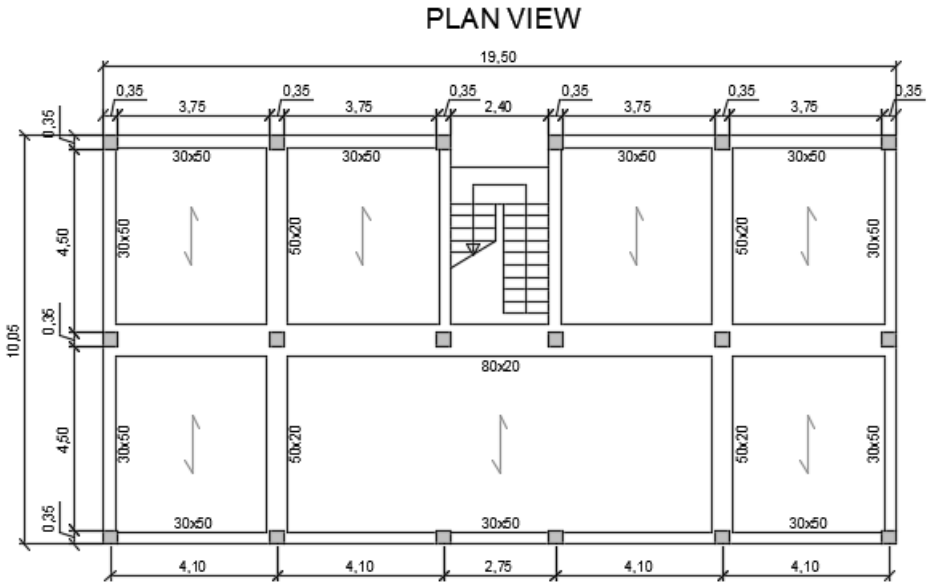

Figure 16. Geometric characteristics of the considered building in terms of plan view.

Funded by the European Union

This project has received funding from the European Union under the Horizon Europe Research & Innovation Programme (Grant Agreement no. 101123467 MultiCare). Views and opinions expressed are however those of author(s) only and do not necessarily reflect those of the European Union. Neither the European Union nor the granting authority can be held responsible for them.

Table 4. Mechanical characteristics of materials

Mechanical property	Symbol	Value
Concrete compressive strength	f'_c [MPa]	20.00
Concrete peak strain	ε'_c [---]	0.0020
Concrete ultimate strain	ε_{cu}	0.0035
Steel yielding stress	f'_y [MPa]	430.00
Steel ultimate stress	f'_u [MPa]	540.00
Steel modulus of elasticity	E_s [GPa]	210.00
Steel ultimate strain	ε_{su}	0.0040

4.2. Modelling approach for the as-built configuration

Building on the information related to the case study, a seismic assessment has been carried out. More specifically, a non-linear static pushover analysis has been performed. The numerical model has been implemented in the software SAP2000 for Finite Element Modelling (FEM). More specifically, a lumped plasticity approach has been adopted, and mono-dimensional frame elements with plastic hinges at the end sections have been used for modelling structural components. Both for beams and columns, the plastic hinges' behaviour is modelled through moment-curvature relationships, and the plastic hinges' length is defined according to Priestley et al. 2007. The shear and shear/flexure failures have also been considered by following the instructions of the New Zealand Society of Earthquake Engineering (NZSEE, 2017) guidelines for seismic assessment of existing buildings. Concerning the hysteretic behaviour, as in the case of past research works (e.g., Molitierno et al. 2023), the Pivot model available in SAP2000 has been used, and the parameters adopted can be found in Table 5.

Table 5. Modelling assumptions and considered parameters for hysteresis rules.

Member	Non-linear Element	Hysteresis Model	Parameters
Columns	Frame with plastic hinges at the end sections	Pivot	α_1=10 α_2=10 β_1=1 β_2=1 η=0.8
Beams	Frame with plastic hinges at the end sections	Pivot	α_1=10 α_2=10 β_1=1 β_2=1 η=0.9
External Beam-Column Joints	Rotational Springs	Pivot	α_1=1 α_2=1 β_1=0.15 β_2=0.15 η=0.8
Internal Beam-Column Joints	Rotational Springs	Pivot	α_1=0.5 α_2=0.5 β_1=0.15 β_2=0.15 η=0.8
Infills	Axial Spring (compression only)	Pivot	α_1=0 α_2=0.25 β_1=0 β_2=0 η=0

Beam-column joints have been modelled by using a system of rigid links and rotational springs. The moment-shear deformation relationship has been defined by following the

Funded by the European Union

This project has received funding from the European Union under the Horizon Europe Research & Innovation Programme (Grant Agreement no. 101123467 MultiCare). Views and opinions expressed are however those of author(s) only and do not necessarily reflect those of the European Union. Neither the European Union nor the granting authority can be held responsible for them.

instructions available in NZSEE 2017. As in the case of beams and columns, the hysteretic behaviour has been modelled using the Pivot model.
Concerning masonry infills, a single strut model has been considered. Each infill panel has been modelled using two links working only in compression. The shear-displacement relationship proposed by Panagiotakos & Fardis 1996 has been adopted to model the response of the infill. A tri-linear force-displacement relationship considering the cracking, peak, and residual strength has been derived for each infill panel. The hysteretic behaviour, as in the previous cases, has been modelled by using the Pivot model. The Pivot parameters adopted (available in Table 5) have been defined according to Molitierno et al. 2023, who defined such parameters according to the results of previous experimental tests on infilled frame systems.
Finally, for the sake of simplicity, soil-structure interaction has been neglected, and fixed-base connections have been assumed. A schematic representation of the adopted modelling approach is provided in Fig. 15.

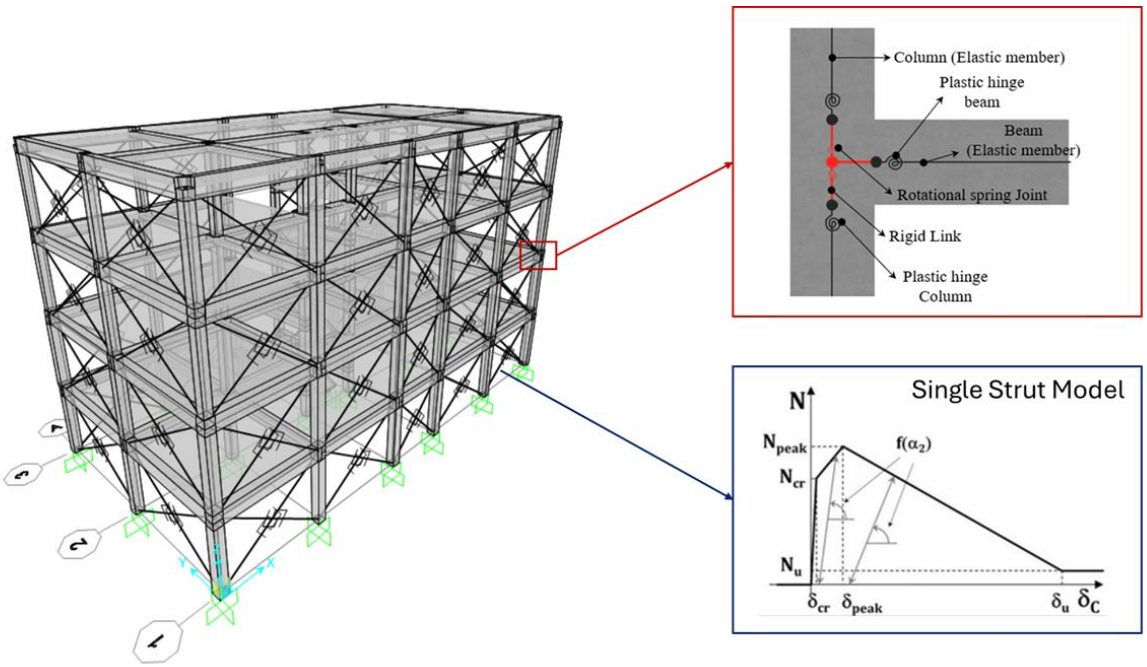

Figure 17. Modelling approach for existing RC infilled frame buildings. Modified after Molitierno et al. 2023 and D'Amore & Pampanin 2025.

Non-linear static analyses have been performed neglecting the second-order effects (i.e., the P-Δ effects). Such a choice is justified by the relatively limited drift demand and considering the relatively reduced height of the building (i.e., a 4-story building). For non-linear static analyses, a load distribution proportional to the story masses has been considered.

4.3. Evaluation of the seismic performance for the as-built configuration

Seismic performance was evaluated through non-linear static (push-over) analyses. For the sake of brevity, only the results related to the longitudinal direction are presented. First, a pushover analysis has been implemented for the RC infilled frame building in the as-built configuration (Figure 18a). In this case, the failure mechanism is governed by shear failures in columns due to the interaction with masonry infills. More specifically, since the numerical models have been implemented by using a single-strut approach (i.e., not able to assess the local interaction between structural and non-structural components), an a-posteriori evaluation was conducted to assess such an interaction. Following an approach analogous

Funded by the European Union

This project has received funding from the European Union under the Horizon Europe Research & Innovation Programme (Grant Agreement no. 101123467 MultiCare). Views and opinions expressed are however those of author(s) only and do not necessarily reflect those of the European Union. Neither the European Union nor the granting authority can be held responsible for them.

to that presented in Di Trapani et al. (2023), it was possible to consider the shear acting on the column as the sum of the drift-related shear acting on the frame and the additional shear demand induced by the interaction with the infill. The latter can be considered as a portion of the horizontal component of the force acting on the strut, and more specifically, only the rate transmitted to the column through horizontal normal stresses, depurated by the portion transferred through shear stresses between the top of the infill and the intrados of the beam. On the other hand, the shear capacity of the columns was evaluated using the model available in the NZSEE 2017 guidelines, and such a capacity was compared to the demand to define the step of the analysis where the failure occurred.

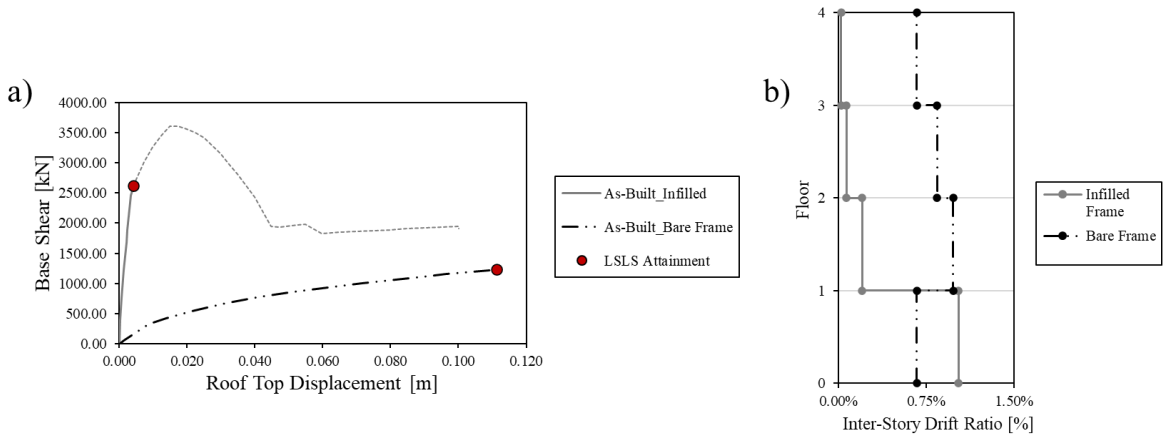

Figure 18. a) PushOver analyses and b) inter-storey drift profile at the attainment at the LSLS for the as-built structure in the infilled configuration (grey line) and considering the selective weakening approach for decoupling masonry infills (black line).

A second analysis was thus carried out by neglecting the effect of the infills, thus reflecting the effect of the selective weakening approach. Such an approach aims at decoupling the masonry infills from the surrounding RC frame before the installation of the exoskeleton. The selective weakening approach is adopted to enhance the seismic performance of existing non-structural components. This involves increasing the in-plane capacity of masonry walls by making vertical and horizontal cuts at the interface between the infills and the RC frame (Figure 19). The gaps are then filled using soft materials, as elastomers. This system allows for eliminating the interaction until the gap closure, thus drastically reducing expected damage in infills and RC structural components due to the interaction. In the specific case, a 3cm gap has been considered, thus ensuring a decoupled behaviour up to 1% drift.

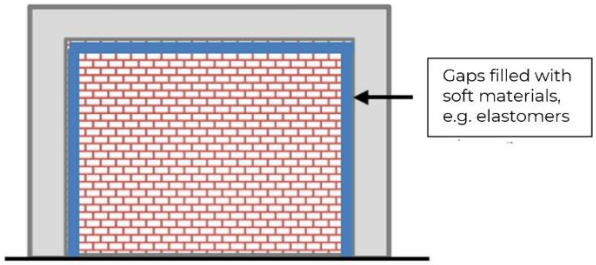

Figure 19. Provision of a gap for decoupling the infills from the surrounding RC frame structure.

Looking at the results of such an analysis (Figure 18a), it is possible to note that the shear failures in columns are prevented, and the as-built structure presents a more desirable ductile behaviour, even if a remarkable reduction of strength and stiffness is observed.

Funded by the European Union

This project has received funding from the European Union under the Horizon Europe Research & Innovation Programme (Grant Agreement no. 101123467 MultiCare). Views and opinions expressed are however those of author(s) only and do not necessarily reflect those of the European Union. Neither the European Union nor the granting authority can be held responsible for them.

Moreover, looking at the results in terms of drift at the attainment of the LSLS (Figure 18b), it is possible to note that in the case of the selective weakening approach, there is a regularisation of the seismic response. Indeed, rather than having a concentration of damage on the first floor (infilled frame), the selective weakening approach allows for having a behaviour close to that of a bare frame structure, which helps redistribute inelasticity along the height.
Building on the results of the aforementioned analyses, it was possible to assess the Safety Index IS-V (defined as the ratio between the capacity and the demand at the LSLS, according to the "*Italian Guidelines for Seismic Risk Classification of Constructions*", Cosenza et al., 2018. Such a value is equal to 52% in the case of the infilled frame, and increases to 75% when the selective weakening approach is implemented, thus further confirming the beneficial effect of decoupling masonry infills in existing structures, Figure 20.

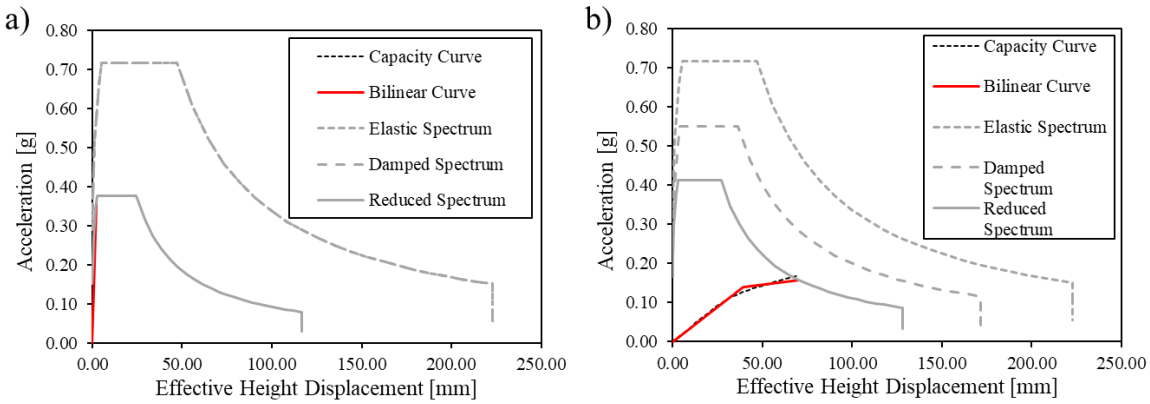

Figure 20. Comparison between the seismic capacity and demand within the ADRS spectrum for the as-built structure in a) the infilled frame configuration, and b) in the case of implementation of the selective weakening approach.

Table 6. Defined IS-V values for the as-built configurations, both for the infilled frame and the case of the selective weakening approach.

Configuration	IS-V
As-Built, Infilled Frame	52%
As-Built, Selective Weakening	75%

4.4. Application of the Displacement-Based Retrofit Procedure

This paragraph illustrates the application of the DBR procedure to design the Pres-Lam exoskeleton. Specifically, in the following, the application of the DBR for the DCLS (§4.4.1) and for the LSLS (§4.4.2) has been differentiated.

4.4.1. Application of the DBR procedure at the DCLS

Building on the results of the seismic assessment of the as-built structure, the DBR procedure at the DCLS has been implemented. Concerning the exoskeleton, a Pres-Lam frame system, characterised by both beams and columns 68cm x 32cm, has been considered. Concerning the material properties of the exoskeleton, a Glulam GL30C has been considered. The mechanical characteristics of the selected material are summarised in Table 7.

Funded by the European Union

This project has received funding from the European Union under the Horizon Europe Research & Innovation Programme (Grant Agreement no. 101123467 MultiCare). Views and opinions expressed are however those of author(s) only and do not necessarily reflect those of the European Union. Neither the European Union nor the granting authority can be held responsible for them.

The limit drift at the DCLC, θ_{DCLS}, is equal to 0.43%. Such a value is imposed by the equivalent yielding point of the as-built structure, where the selective weakening approach is implemented. In any case, by comparing the capacity spectrum of the as-built structure with the seismic demand at the DCLS, it was observed, for the specific case, that the as-built structure was already verified for such a limit state, as illustrated in Figure 21.

Table 7. Mechanical characteristics of the Glulam GL30C

Mechanical property	Symbol	Value
Strength in compression parallel to the grain	$f_{c,0,g,k}$ [MPa]	24.50
Modulus of elasticity parallel to the grain	$E_{0,g,Mean}$ [MPa]	13000
Modulus of elasticity perpendicular to the grain	$E_{90,g,Mean}$ [MPa]	300
Shear Modulus	$G_{g,Mean}$ [MPa]	650
Density	$\rho_{g,Mean}$ [kg/m3]	430

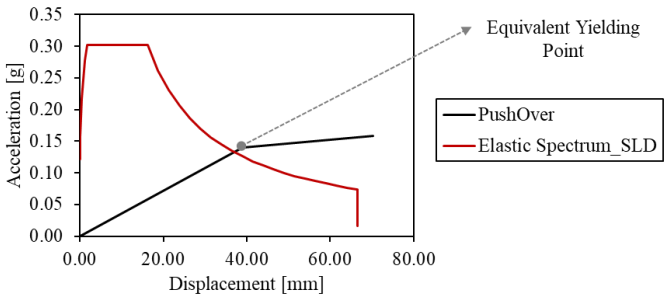

Figure 21. Comparison between the seismic capacity and demand at the DCLS for the as-built structure, considering the implementation of the selective weakening approach.

For this reason, to further enhance the stiffness of the retrofitted structure, a reduced design drift equal to 0.30% has been selected. Such a design drift, $\theta_{D,DCLS}$, allows to define the displacement profile by using Equation 21, which considers a linear deformed shape for the retrofitted building:

$$\Delta_i = \theta_{D,DCLS} \cdot H_i \tag{21}$$

Where H_i represents the height of the *i*-th storey. Once the displacement profile is determined, the crucial parameters of displacement-based procedures (i.e., Δ_D, m_{Eff}, and H_{Eff}) can be defined by using Equations 12, 13, and 14. In any case, it is worth stressing that the $\theta_{D,DCLS} = 0.30\%$ value is an initial guess in the procedure. Indeed, after defining the internal actions with the DBR, and the associated deformation at components level, the total elastic deformation θ_y should be computed by using Equation 2. The iterative procedure ends when $\theta_{D,DCLS} = \theta_y$. For the sake of brevity, only the results related to the final iteration, corresponding to a $\theta_{D,DCLS} = 0.28\%$ are reported in this document.

This project has received funding from the European Union under the Horizon Europe Research & Innovation Programme (Grant Agreement no. 101123467 MultiCare). Views and opinions expressed are however those of author(s) only and do not necessarily reflect those of the European Union. Neither the European Union nor the granting authority can be held responsible for them.

Table 8. Parameters of the DBR at the DCLS.

Level	m_i [Ton]	H_i [m]	Δ_i [m]	$m_i\Delta_i$	$m_i\Delta_i^2$	$m_i\Delta_i H_i$
1	194.53	3.10	0.009	1.773	0.016	5.50
2	192.78	6.20	0.018	3.514	0.064	21.79
3	186.22	9.30	0.027	5.091	0.139	47.35
4	148.87	12.40	0.036	5.427	0.198	67.29

$$\Delta_D = \frac{\sum_{i=1}^{N}(m_i\Delta_i)^2}{(m_i\Delta_i)} = 0.026\ m$$

$$m_{Eff} = \frac{\sum_{i=1}^{N}(m_i\Delta_i)}{\Delta_d} = 598.68\ Ton$$

$$H_{Eff} = \frac{\sum_{i=1}^{N}(m_i\Delta_i h_i)}{(m_i\Delta_i)} = 8.98\ m$$

Once the design displacement, Δ_D, has been defined, it is possible to determine the effective period, T_{Eff}, from the elastic spectrum at the DCLS (5%-damped). Using the effective period T_{Eff}, the effective stiffness, K_{Eff}, together with the total base shear, V_{Tot}, and the base shear carried out by the exoskeleton, V_{Exo}, can be defined:

$$K_{Eff} = m_{Eff}\left(\frac{2\pi}{T_{Eff}}\right)^2 = 41344.94\ kN/m$$

$$V_{Tot} = K_{Eff} \cdot \theta_{D,DCLS} = 1162.64\ kN$$

$$V_{Exo} = V_{Tot} - V_{AsBuilt} = 640.10kN \Rightarrow 320.05kN \text{ for each exoskeleton}$$

The base shear is then distributed in proportion to floor masses and displacement, with an additional 10% at the roof level to account for additional storey shear resulting from higher modes effects, Equation 22.

$$\frac{\mathrm{F_i}}{\mathrm{V_{Base}}} = 0.1_{\mathrm{i=N}} + 0.9\frac{m_i\Delta_i}{\sum_{i=1}^{N}(m_i\Delta_i)} \quad (22)$$

Table 9. DCLS: Distribution of base shear. V_S: Storey shear.

Level	F_i [kN]	F [kN]	V_S [kN]	F_iH_i [kNm]
1	0.101	32.31	320.05	100.16
2	0.200	64.04	287.74	397.04
3	0.290	92.79	223.70	862.95
4	0.409	130.91	130.91	1623.29

Funded by the European Union

This project has received funding from the European Union under the Horizon Europe Research & Innovation Programme (Grant Agreement no. 101123467 MultiCare). Views and opinions expressed are however those of author(s) only and do not necessarily reflect those of the European Union. Neither the European Union nor the granting authority can be held responsible for them.

The earthquake induced axial load, is determined from the overturning moment demand ($OTM = \sum_{i=1}^{N} F_i H_i$) and the geometry of the exoskeleton, Equation 23.

$$N_E = \frac{\sum_{i=1}^{N} F_i H_i - V_{Exo} \cdot \gamma H_i}{L_{Base}} = 129.30\ kN \tag{23}$$

Here N_E stands for the earthquake-induced axial load on the ground floor external columns, while γ is a design parameter related to the position of the contraflexure point in the columns at the ground level. Such a value is typically taken equal to 0.60, thus ensuring that hinging does not occur at the top of the ground floor columns. L_{Base} is the length of the exoskeleton.
The beam shear $V_{b,i}$, Equation 24, is distributed up the height of the building, proportioned based on the storey shear at each level, $V_{S,i}$.

$$V_{b,i} = N_E \cdot \frac{V_{S,i}}{\sum_{i=1}^{N} V_{S,i}} \tag{24}$$

The beam positive and negative moment $M_{b,i}$ can be easily determined from Equation 25, while the design moment at the column interface $M^*_{b,i}$ is defined from Equation 26.

$$M_{b,i} = \frac{V_{b,i} L_b}{2} \tag{25}$$

$$M^*_{b,i} = \frac{V_{b,i} L_b}{2}\left(1 - \frac{h_c}{L_b}\right) \tag{26}$$

Once $M^*_{b,i}$ is determined, it is possible to define the post-tension force, T_{PT} (Equation 5), and all the deformation at the components level (Equations from 6 to 10).

Table 10. DCLS: Definition of deformations at components level for interior elements.

Level	$V_{b,i}$ [kN]	$M_{b,i}$ [kNm]	$M^*_{b,i}$ [kNm]	T_{PT} [kN]	θ_b	θ_c	θ_j	θ_{int}	$\theta_{y,i}$
1	43.00	88.15	73.53	205.00	0.07%	0.10%	0.18%	0.13%	0.46%
2	38.66	79.25	66.11	185.00	0.06%	0.09%	0.16%	0.11%	0.41%
3	30.05	61.61	51.39	145.00	0.05%	0.07%	0.13%	0.09%	0.32%
4	17.59	36.06	30.08	85.00	0.03%	0.04%	0.08%	0.05%	0.19%

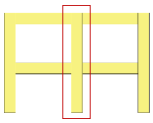

Funded by the European Union

This project has received funding from the European Union under the Horizon Europe Research & Innovation Programme (Grant Agreement no. 101123467 MultiCare). Views and opinions expressed are however those of author(s) only and do not necessarily reflect those of the European Union. Neither the European Union nor the granting authority can be held responsible for them.

Table 11. DCLS: Definition of deformations at components level for exterior elements.

Level	$V_{b,i}$ [kN]	$M_{b,i}$ [kNm]	$M^*_{b,i}$ [kNm]	T_{PT} [kN]	θ_b	θ_c	θ_j	θ_{int}	$\theta_{y,i}$
1	43.00	88.15	73.53	205.00	0.07%	0.05%	0.13%	0.13%	0.36%
2	38.66	79.25	66.11	185.00	0.06%	0.05%	0.12%	0.11%	0.32%
3	30.05	61.61	51.39	145.00	0.05%	0.04%	0.09%	0.09%	0.25%
4	17.59	36.06	30.08	85.00	0.03%	0.02%	0.06%	0.05%	0.15%

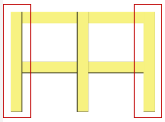

Building on these results, it is possible to define the total elastic deformation of the exoskeleton, and check if this value is minor than the limit drift defined at the beginning of the procedure itself (i.e., 0.43%).

$$\theta_y = \frac{\sum_{i=1}^{N} M_{con\,i,DCLS}\theta_{y,i}}{\sum_{i=1}^{N} M_{con\,i,DCLS}} = 0.28\% < 0.43\% \Rightarrow Check\ OK!$$

4.4.2. Application of the DBR procedure at the LSLS

Concerning the implementation of the DBR at the LSLS, the design drift is defined based on the seismic assessment of the retrofitted structure as follow:

$$\theta_D = \frac{\Delta_{Max,AB}}{H_{Eff,AB}} = 0.78\%$$

As in the case of the DBR procedure at the DCLS, the procedure at the LSLS is also iterative. Because it is used to design the exoskeleton, some data can only be specified as an initial guess at the beginning, as they are determined by the design process itself. Specifically, the post-yield stiffness ratio r, and the ratio between the shear carried out by the exoskeleton and that carried out by the as-built structure, $V_{Exo}/V_{As,Built}$. As done in the previous case, for the sake of brevity, only the results related to the last iteration are summarised in this document.

In order to define the effective period of the retrofitted building, this must be converted into a Single Degree of Freedom (SDoF) system. To do this, several parameters associated with the Multi Degree of Freedom (MDoF) system must be calculated using Equations from 12 to 14. These are all based on the design displacements at each level, which are calculated by using Equation 27:

$$\Delta_i = \delta_i \left(\frac{\Delta_c}{\delta_c}\right) \tag{27}$$

In this equation, δ_i is the displacement shape factor at each level, Δ_c (Equation 28) is the displacement at the critical level (i.e., first floor for frame systems), and δ_c is the shape factor at the critical level, Figure 22.

$$\Delta_c = \theta_D H_{i=1} \tag{28}$$

Funded by the European Union

This project has received funding from the European Union under the Horizon Europe Research & Innovation Programme (Grant Agreement no. 101123467 MultiCare). Views and opinions expressed are however those of author(s) only and do not necessarily reflect those of the European Union. Neither the European Union nor the granting authority can be held responsible for them.

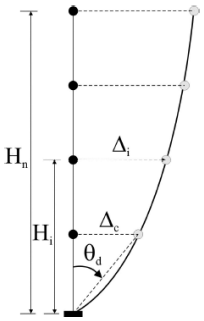

Figure 22. Inelastic displaced shape of a frame structure (NZSC, 2010)

Concerning the displacement shape factor δ_i, alternative formulations (Equations 29 and 30) can be adopted depending on the total number of storeys.

$$\delta_i = \frac{H_i}{H_N} \quad \Rightarrow \quad N \leq 4 \tag{29}$$

$$\delta_i = \frac{4}{3} \cdot \left(\frac{H_i}{H_N}\right) \cdot \left(1 - \frac{H_i}{4 \cdot H_N}\right) \quad \Rightarrow N > 4 \tag{30}$$

Where H_i is the level of the i-th floor, and H_N is the level of the roof (i.e., total height of the building). Since in the specific case, the considered building is a 4-storey building, the linear function (Equation 29) for the displacement shape factor has been adopted.

Table 12. Parameters of the DBR at the LSLS.

Level	m_i [Ton]	H_i [m]	Δ_i [m]	$m_i\Delta_i$	$m_i\Delta_i^2$	$m_i\Delta_i H_i$
1	194.53	3.10	0.024	4.715	0.114	14.62
2	192.78	6.20	0.048	9.346	0.453	57.94
3	186.22	9.30	0.073	13.541	0.985	125.94
4	148.87	12.40	0.097	14.434	1.399	178.98

$$\Delta_D = \frac{\sum_{i=1}^{N}(m_i\Delta_i)^2}{(m_i\Delta_i)} = 0.070\ m$$

$$m_{Eff} = \frac{\sum_{i=1}^{N}(m_i\Delta_i)}{\Delta_d} = 598.68\ Ton$$

$$H_{Eff} = \frac{\sum_{i=1}^{N}(m_i\Delta_i h_i)}{(m_i\Delta_i)} = 8.98\ m$$

The equivalent viscous damping ξ of the system is defined through Equation 15, and takes into account both the equivalent viscous damping associated with the as-built structure ξ_{AB}, and the one related to the exoskeleton ξ_{Exo}.

$$\xi_{AB} = k\frac{63.7\left(a_y^* d_{max}^* - a_{max}^* d_y^*\right)}{a_{max}^* d_{max}^*} + 5 = 11.92\%$$

This project has received funding from the European Union under the Horizon Europe Research & Innovation Programme (Grant Agreement no. 101123467 MultiCare). Views and opinions expressed are however those of author(s) only and do not necessarily reflect those of the European Union. Neither the European Union nor the granting authority can be held responsible for them.

Concerning ξ_{Exo}, this value is dependent on the ductility μ of the exoskeleton, and the post-yield stiffness ratio r. The first value is calculated as the ratio between the design drift and the total elastic deformation of the frame:

$$\mu = \frac{\theta_D}{\theta_y} = 2.82$$

As anticipated before, the r factor is a variable of the design procedure. In this specific case, at the last iteration $r = 0.11$. In any case, it is worth noticing that acceptable values of the r factor for Pres-Lam timber structure should be close to 0.10, as in the specific case. Considering these values, ξ_{Exo} can be easily determined.

$$\xi_{Exo} = 5\% \cdot \mu^{-0.43} + 0.65 \cdot \frac{(2-2\beta)(\mu-1)}{\mu\pi\left(1+r(\mu-1)\right)} = 11.25\%$$

Once ξ_{AB} and ξ_{Exo} are determined, ξ can be calculated. Here it should be highlighted that this value is dependent on both the base shear carried out by the exoskeleton and the one carried out by the as-built structure. Since the exoskeleton must be designed, at this stage of the procedure is not possible to know exactly the base shear carried out by the exoskeleton. Consequently, the ratio $V_{Exo}/V_{As,Built}$ should be considered as a variable in the design process. At the last iteration, such value is equal to 0.83.

$$\xi = \frac{\xi_{AB} V_{B,AB} + \xi_{Exo} V_{B,Exo}}{V_{B,AB} + V_{B,Exo}} = 11.62\%$$

Using the equivalent viscous damping, it is possible to define the damped displacement spectrum, which can be defined by calculating the factor R_ξ.

$$R_\xi = \sqrt{\frac{10}{5+\xi}} = 0.78$$

Using the damped spectrum and the design displacement Δ_D, the effective period T_{Eff} can be determined, together with all the others important parameters allowing to define the base shear, the internal actions, and finally designing the exoskeleton. Since from this point on, all the calculations are identical to those presented before in §4.4.1, only the results are summarized in the following:

$$K_{Eff} = m_{Eff}\left(\frac{2\pi}{T_{Eff}}\right)^2 = 24168.29\ kN/m$$

$$V_{Tot} = K_{Eff} \cdot \theta_{D,DCLS} = 1696.96\ kN$$

$$V_{Exo} = V_{Tot} - V_{AsBuilt} = 767.12\ kN \Rightarrow 383.56\ kN \text{ for each exoskeleton}$$

Funded by the European Union

This project has received funding from the European Union under the Horizon Europe Research & Innovation Programme (Grant Agreement no. 101123467 MultiCare). Views and opinions expressed are however those of author(s) only and do not necessarily reflect those of the European Union. Neither the European Union nor the granting authority can be held responsible for them.

Table 13. LSLS: Distribution of base shear. V_S: Storey shear.

Level	F_i [kN]	F [kN]	V_S [kN]	F_iH_i [kNm]
1	0.101	38.72	383.56	120.04
2	0.200	76.75	344.84	475.83
3	0.290	111.20	268.09	1034.19
4	0.409	156.89	156.89	1945.42

$$N_E = \frac{\sum_{i=1}^{N} F_i H_i - V_{Exo} \cdot \gamma H_i}{L_{Base}} = 152.08\ kN$$

Table 14. LSLS: Internal actions distribution, derived using the equilibrium method

Level	$V_{b,i}$ [kN]	$M_{b,i}$ [kNm]	$M^*_{b,i}$ [kNm]
1	50.57	103.68	86.48
2	45.47	93.21	77.75
3	35.35	72.46	60.45
4	20.69	42.41	35.37

Finally, the moment at the base of the columns at ground floor, have been computed by using a simplified method, as reported in Equation 31.

$$M_{Col} = \gamma H_{Int} V_{Exo} = 118.90\ kNm \quad (31)$$

4.4. Section design

A step-by-step general design procedure which described the response of post-tensioned dry jointed ductile connection was initially developed and proposed by Pampanin et al. (Pampanin et al., 2001). This design procedure was based upon a Monolithic Beam Analogy (MBA), used to describe the complete moment-rotation behaviour of the connection. In the calculation of the moment-rotation response of a post-tensioned timber jointed ductile connection of a Pres-Lam exoskeleton, the same basic principles are followed as those applied to reinforced concrete, however some minor alterations must be made. Specifically, it is required that strains in the timber (Equation 31) remain below the materials yield strain and therefore the pre-yield form of the MMBA is used in design:

$$\varepsilon_t = c\left(3\frac{\theta_{imp}}{L_{cant}} + \phi_{dec}\right) \quad (31)$$

In the equation above, ε_t is the strain at the extreme fibre of the timber beam, L_{cant} the distance from the interface to the point of contra-flexure, and ϕ_{dec} the decompression curvature. A triangular stress block can be used for timber as it remains below the yield strain.

This project has received funding from the European Union under the Horizon Europe Research & Innovation Programme (Grant Agreement no. 101123467 MultiCare). Views and opinions expressed are however those of author(s) only and do not necessarily reflect those of the European Union. Neither the European Union nor the granting authority can be held responsible for them.

The general procedure of the section design is illustrated in Figure 23, while the characteristics of the beam section considered in this case-study application are shown in Figure 24.

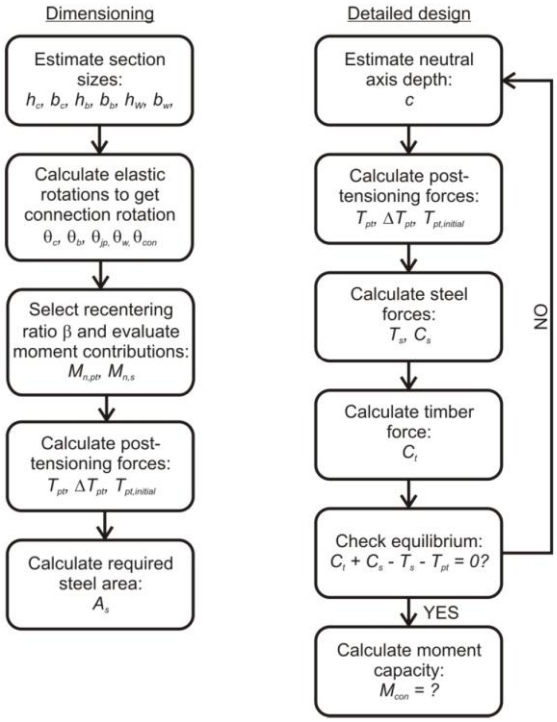

Figure 23. Summary of post-tensioned timber design procedure.

Specifically, in this design example an exterior joint is considered.

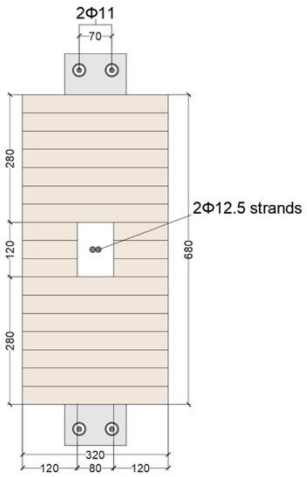

Post-tensioning tendons	
2-12.5 strands	
Total Area, A_{pt}	186 mm^2
Initial post-tensioning force	205 kN
Mild steel reinforcement	
4-11 mm diameter bars	
Steel yield stress, f_y	275 MPa
Edge distance, $y_{s,c}$	50 mm

Figure 24. Section size and detailing.

First, the interface compression rotation when the decompression occurs, as already anticipated in the previous Chapter and expressed in Equation 9, is calculated equal to

This project has received funding from the European Union under the Horizon Europe Research & Innovation Programme (Grant Agreement no. 101123467 MultiCare). Views and opinions expressed are however those of author(s) only and do not necessarily reflect those of the European Union. Neither the European Union nor the granting authority can be held responsible for them.

$$\theta_{int} = k_{int}\frac{2T_{pt,initial}h_c}{E_{perp}{h_b}^2 b_b} = 0.13\%$$

The joint rotation is equal to

$$\theta'_{con} = \theta_d - \theta_b - \theta_c - \theta_j = 0.78\% - 0.08\% - 0.06\% - 0.16\% = 0.48\%$$

Where θ_d is the design target drift, imposed as 0.78%, while θ_b, θ_c *and* θ_j are expressed by Equation 6, 7a, 7b, 8a, 8b, respectively.
The connection rotation becomes:

$$\theta_{con} = \frac{\theta_{con}}{\left(1 - \frac{h_c}{L_b}\right)} = 0.58\%$$

Therefore, the imposed rotation is the following:

$$\theta_{imp} = \theta_{con} - \theta_{int} = 0.45\%$$

In order to obtain the equilibrium, the neutral axis value is:

$$c = 0.15$$

From this value, the force in the post-tensioning is calculated as the increase in strain due to gap opening added to the original post-tensioning force:

$$T_{pt} = T_{pt,initial} + \Delta T_{pt}$$

$$\Delta_{pt} = \theta_{imp}\left(y_{pt} - c\right) = 0.78\ mm$$

$$\Delta\varepsilon_{pt} = \frac{n_{gap}\Delta_{pt}}{l_{ub}} = 0.03\%$$

$$\Delta T_{pt} = \Delta\varepsilon_{pt}E_{pt}A_{pt} = 24.38\ kN$$

Therefore,

$$T_{pt} = T_{pt,initial} + \Delta T_{pt} = 229.38\ kN$$

In the equations above, n_{gap} is the number of gap interfaces along the entire frame length, and E_{pt} is the elastic modulus of the post-tensioned tendons.
As far as the external Plug&Play dissipaters are concerned, the elongation in tension and compression is defined as follows:

$$\Delta_{s,t} = \theta_{imp}\left(y_{s,t} - c\right) = 2.08\ mm$$
$$\Delta_{s,c} = \theta_{imp}\left(c - y_{s,c}\right) = 0.53\ mm$$

Knowing the length of the dissipaters fuse, L_{fuse}, the strain can be calculated:

$$\varepsilon_{s,t} = \frac{\Delta_{s,t}}{L_{fuse}} = 1.26\%$$
$$\varepsilon_{s,t} = \frac{\Delta_{s,c}}{L_{fuse}} = 0.32\%$$

The stressed and foce in the dissipaters are now calculated:

Funded by the European Union

This project has received funding from the European Union under the Horizon Europe Research & Innovation Programme (Grant Agreement no. 101123467 MultiCare). Views and opinions expressed are however those of author(s) only and do not necessarily reflect those of the European Union. Neither the European Union nor the granting authority can be held responsible for them.

$$f_s = f_y + \left[1 + r\left(\frac{\varepsilon_s}{\varepsilon_y} - 1\right)\right]$$

$$f_{s,t} = 293.77\ MPa$$
$$f_{s,c} = 277.95\ MPa$$

$$T_s = A_s f_{s,t} = 55.84\ MPa$$

$$C_s = A_s f_{s,c} = 52.83\ MPa$$

Where, *r* is the strain hardening ratio considered equal to 0.8 % in this design example as a reasonable approximation to the post-yield stress of mild steel.
As already anticipated at the beginning of the paragraph, the elastic range of MMBA is now used to calculate the timber strain (Equation 31), which has to be lower than the maximum strain depending on the type of timber used. In this application, a Glulam Gl30c has been chosen, characterized by a compression strength parallel to the grain f_c equal to 24.5 and a modulus of elasticity parallel to the grain $E_{t,par}$ equal to 13 GPa:

$$\varepsilon_t = 0.12\% \leq \frac{f_c}{k_{gap} E_{t,par}} = 0.34\% \rightarrow CHECK\ OK$$

In this equation, k_{gap} is defined by the grade of reinforcement perpendicular to the grain within the beam-column joint. In this application a k_{gap} equal to 0.55 has been used, as epoxied rods have been inserted within the column (refer to Table 3).
Knowing the strain in timber and assuming a triangular timber stress block the compression force in timber is calculated:

$$C_t = 0.5 k_{gap} \varepsilon_t E_{t,par} b_b c = 224.49$$

The equilibrium is checked:

$$-C_t - C_s + T_s + T_{pt} = 7.9 \approx 0 \rightarrow CHECK\ OK$$

The moment is now calculated about the centroid of the timber member

$$M_{con} = \left[C_t\left(\frac{h}{2} - \frac{c}{3}\right) + T_s\left(y_{s,t} - \frac{h}{2}\right) + C_s\left(\frac{h}{2} - y_{s,c}\right)\right] = 97.54\ kNm$$

Finally, the re-centering ratio β is checked:

$$\beta = \frac{M_{pt}}{M_{con}} = \frac{T_{pt}\left(y_{pt} - \frac{c}{3}\right)}{M_{con}} = 0.67 \approx 0.60 \rightarrow CHECK\ OK$$

4.5. Modelling approach and evaluation of the seismic performance for the retrofitted configuration

Building on the results of the DBR procedure and of the detailed connection design, the considered exoskeleton is composed of structural members 68 cm in height and 32 cm in width, both for columns and beams.
After designing the exoskeleton, another numerical model of the retrofitted configuration has been implemented. More specifically, in this case, the exoskeleton has been connected in parallel to the as-built structure using rigid links representative of the connection systems between the two structures. Concerning the exoskeleton, in order to model the non-linearities, rather than using plastic hinges, nonlinear links working in parallel at the end sections of structural members have been used, as suggested by Pampanin et al. [30].

Funded by the European Union

This project has received funding from the European Union under the Horizon Europe Research & Innovation Programme (Grant Agreement no. 101123467 MultiCare). Views and opinions expressed are however those of author(s) only and do not necessarily reflect those of the European Union. Neither the European Union nor the granting authority can be held responsible for them.

Such links are modelled to catch the self-centring behaviour of the post-tensioning cables/bars, and the dissipation capabilities related to the Plug&Play dissipaters. More specifically, the multi-linear elastic link has been used for post-tension, while an elastic-plastic one with kinematic hysteresis rule has been adopted for modelling the Plug&Play dissipaters. Finally, an additional rotational spring has been implemented in the system of rigid links, adopted for modelling the beam-column joint, in order to capture the joint shear stiffness (Smith et al., 2014; Di Cesare et al., 2017; Granello et al., 2018). A schematic representation of the modelling approach for the retrofitted configuration is illustrated in Figure 25.

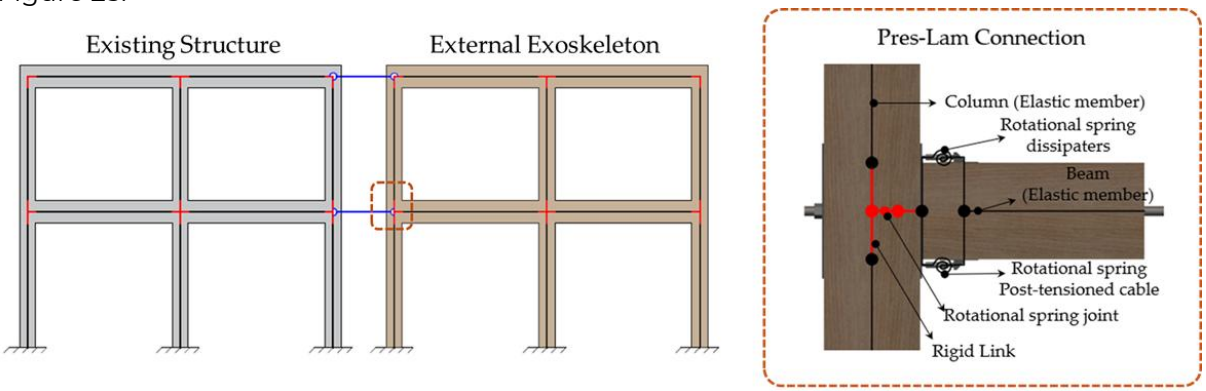

Figure 25. Modelling approach for buildings retrofitted using the low-damage exoskeleton.

Figure 26 presents the results in terms of push-over analysis of the retrofitted structure compared with the as-built configuration (a). Moreover, an additional model of the exoskeleton has been implemented, and non-linear static cyclic analyses have been carried out in order to highlight the peculiar self-centring capabilities of the Pres-Lam exoskeleton (b).

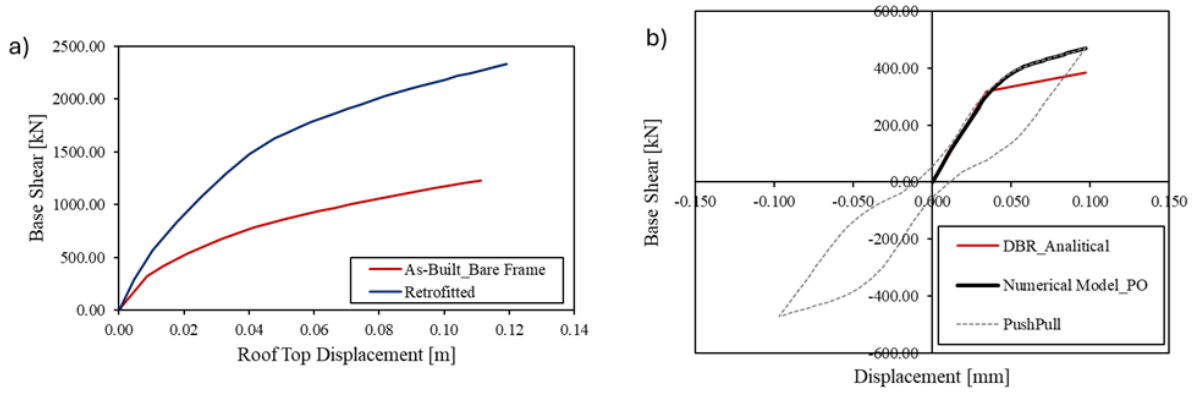

Figure 26. a) Results in terms of push-over curves for the as-built and retrofitted configuration, and b) results of cyclic non-linear static analysis (push-pull) to prove the self-centring capabilities of the external exoskeleton.

Finally, the pushover curve of the retrofitted structure has been converted within the ADRS spectrum, and the Safety-Index, IS-V, has been defined, Figure 27. More specifically, the retrofitted structure scores 120% IS-V, representing a remarkable improvement with respect to the as-built structure, which scored 52% IS-V.

Funded by the European Union

This project has received funding from the European Union under the Horizon Europe Research & Innovation Programme (Grant Agreement no. 101123467 MultiCare). Views and opinions expressed are however those of author(s) only and do not necessarily reflect those of the European Union. Neither the European Union nor the granting authority can be held responsible for them.

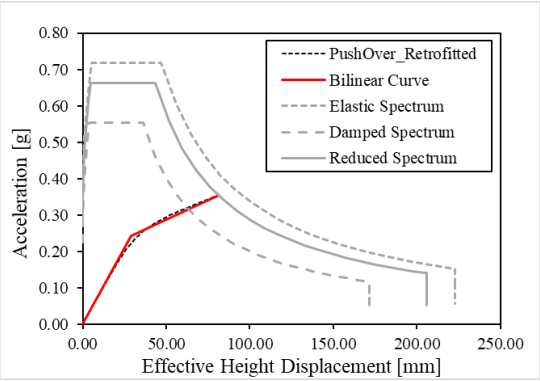

Figure 27. Comparison between the seismic capacity and demand, within the ADRS format, for the retrofitted structure at the LSLS.

5. Connections detailing

5.1 Overview of Pres-Lam connections

Various connection details can be employed within Pres-Lam frames, concerning the type of dissipaters, reinforcement perpendicular to the grain, the arrangement of post-tensioning cables, and the shear key for shear transfer mechanism (Miliziano et al., 2020). As illustrated in Figure 28, a wide range of alternative options can be used for Pres-Lam beam-column joints, many of which have already been successfully implemented in real new-designed buildings around the world. Starting from the post-tensioning reinforcement, bars or strands (Figure 29a) can be alternatively used. Among the Pres-Lam buildings constructed to date using frames as LLRS (i.e., Lateral Load-Resisting System), only one building uses threaded bars (i.e., Beatrice Tinsley building) – which are usually employed in Pres-Lam walls rather than frames.

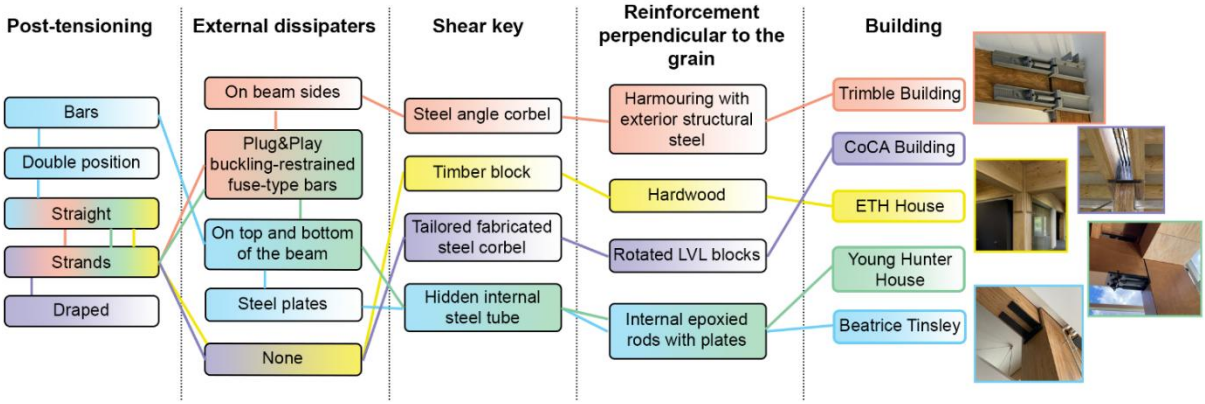

Figure 28. Flowchart outlining the key aspects defining different configurations of Pres-Lam frame connections, and their implementation in buildings constructed to date.

Post-tensioning cables, whether strands or bars, can be placed at the mid-height of the beam and configured in either a straight or draped arrangement. Draped cables are better suited for handling higher gravity loads, reducing the required beam height, while straight tendons are more appropriate for buildings subjected to greater lateral demands, avoiding

Funded by the European Union

This project has received funding from the European Union under the Horizon Europe Research & Innovation Programme (Grant Agreement no. 101123467 MultiCare). Views and opinions expressed are however those of author(s) only and do not necessarily reflect those of the European Union. Neither the European Union nor the granting authority can be held responsible for them.

complicated layout. Alternatively, the post-tensioning reinforcements can run at two different section height, as in the Beatrice Tinsley Building (Figure 29b).

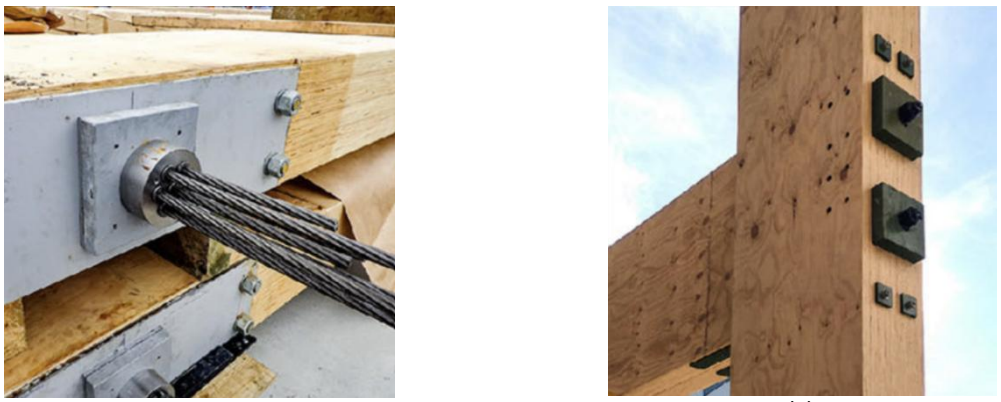

a) b)

Figure 29. a) Post-tensioned strands coming out of the anchorages for post-tensioning in the Young Hunter House building; b) Couple of post-tensioning bars with steel plates anchorage in the Beatrice Tinsley building (Miliziano et al., 2020).

An important concern in Pres-Lam frames is the post-tensioned loss over time due to timber creep. Several research have been investigating this aspect (Davies and Fragiacomo, 2011; Wanninger et al., 2014; Granello et al., 2017), which has been found to largely depend on the perpendicular-to-the-grain compression acting on the column. For this reason, different joint reinforcements have been implemented. In the Trimble Building (Figure 30a), exterior steel armouring on the column - kind of a steel jacketing - is used to bypass the joint, thus allowing to avoid compression perpendicular to grain in the column and reduce the joint deformation. This solution, however, relies on fasteners connecting the plates to the column, which has to be sufficiently stiff. The joint reinforcement in the Young Hunter House (Figure 30b), happens through internal epoxied rods and structural steel plates at the beam-column interface. This solution, however, does not prevent the joint deformation. The CoCA building at Massey University (Figure 30c) uses rotated LVL block glued and bolted to the face of the column, while the ETH House of Natural Resources simply uses hardwood for frame members, thus increasing the column perpendicular to grain strength.

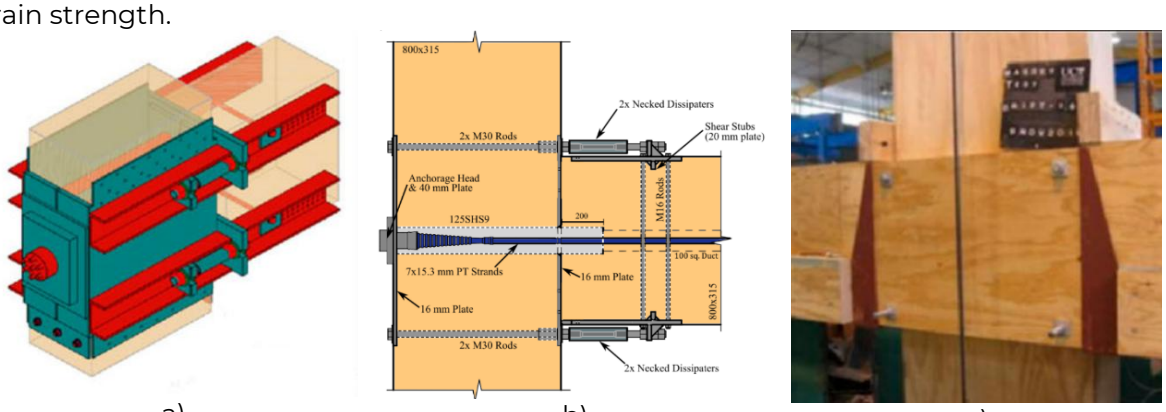

a) b) c)

Figure 30. Column reinforcement perpendicular-to-the-grain using a) exterior column steel jacketing (Brown et al., 2012); b) internal epoxied rods (modified after Horne et al., 2022); c) rotated LVL block (Miliziano et al., 2020).

Funded by the European Union

This project has received funding from the European Union under the Horizon Europe Research & Innovation Programme (Grant Agreement no. 101123467 MultiCare). Views and opinions expressed are however those of author(s) only and do not necessarily reflect those of the European Union. Neither the European Union nor the granting authority can be held responsible for them.

Various energy dissipation devices can be incorporated within hybrid Pres-Lam connections. The Plug&Play buckling-restrained axial tension-compression yielding mild steel bars can be placed on top and bottom of the beam, as in the Young Hunter House, or on its sides as done for the Trimble Building. In both cases, an intermediate plate between timber and the dissipaters should be placed, by using nails and/or bolts. When placed on top and bottom of the beam, the plates fasteners also act as reinforcement perpendicular to grain in the beam. These fasteners, however, must be designed following capacity design principles in order to avoid their failure and timber damage before the failure of the dissipaters. Alternatively, angle steel plates can be used (Beatrice Tinsley Building). This solution involves the use of timber rivets which, however, are not easily removable after a seismic event. When the seismic hazard is low, configurations without any dissipaters can also be considered. Nevertheless, it was found that these devices can absorb the extra moment demand due to post-tensioning losses over time and their use is thus recommended (Granello et al., 2018).
Another key factor that should be taken into account when designing Pres-Lam connection is the shear transfer mechanism at the interface between beam and column. Different solutions can be employed without using any additional device, by considering, for instance, the shear contribution from friction due to the post-tensioning tendons or the dowel actions in the external dissipaters. However, the use of a shear key is recommended. For this purpose, a simple timber solid block (Figure 31a) can be used as a corbel to absorb the shear or, alternatively a steel angle can be placed on the bottom of the beam (Figure 31b). Although these elements are easy to manufacture and install, they can cause damage to timber during the gap opening. For this reason, a small rubber bearing strip should be interposed between the corbel and the beam. Another solution might be represented by a steel tube set within the cavity for post-tensioning into the column and the beam at joint interface (Figure 31c). Even in this case, a gap should be left above the tube so that it can be freely moved up inside the pocket in the column during the rocking motion (Smith, 2014), without causing compression perpendicular to the grain in the beam.

a) b) c)

Figure 31. Different type of shear key: a) Timber solid block on the bottom of the beam (Smith 2008). A similar solution has been implemented in the ETH House of Natural Resources; b) Steel angle as a corbel, Trimble Building; c) Hidden internal steel tube, as in the Young Hunter House and Beatrice Tinsley buildings (modified from van Beerschoten, 2013) .

5.2. Detailed design of Pres-Lam exoskeleton connections

In this paragraph, a case-study application of Pres-Lam connections design will be presented. Specifically, the connection configuration already used within the Young Hunter House (Figure 28) with external dissipaters placed at the bottom and top of the beam section, and centered post-tensioned tendons will be considered, as this configuration ensures the most effective utilization of the devices and it fits properly with the application

Funded by the European Union

This project has received funding from the European Union under the Horizon Europe Research & Innovation Programme (Grant Agreement no. 101123467 MultiCare). Views and opinions expressed are however those of author(s) only and do not necessarily reflect those of the European Union. Neither the European Union nor the granting authority can be held responsible for them.

of a Pres-Lam exoskeleton outside an existing structure. Moreover, a corbel-type shear key will be used. Additional considerations will be made for the column base and top sections. Indeed, post-tensioning tendons must be used even in the columns when employing Pres-Lam frames for the rehabilitation of existing structures through external exoskeletons, since the absence of external axial loads does not sufficiently guarantee a proper re-centering of the low-damage structure.

5.2.1. Beam-column joint design

The connections of the Pres-Lam exoskeleton are designed and verified in accordance with the Eurocodes and the New Zealand Standards for timber and steel. Specifically, the latter is applied to those connection elements not covered within the European standards or when more stringent verification criteria are provided. The code references for the main verification conducted on the connection systems are summarised in Table 15.

Table 15. Codes used for the verification of the structural connections.

Connection System	Code
Dissipaters plates and fasteners: shear resistance	EN 1995-1-1:2004
Dissipaters plates and fasteners: bearing resistance	EN 1993-1-8:2005
Fasteners spacing	EN 1993-1-8:2005
Reinforcement perpendicular to grain	ETA TR 070:20019-10
Shear key	NZS AS 1720.1:2022
Post-tension end-plate	NZS 3404:1997

The technical drawings of the beam-column joint are illustrated in Figure 32. The length of the two external Plug&Play dissipaters (Detail A1 in Figure 32) of the beam, designed as outlined in the previous paragraphs, are characterised by a slenderness ratio l expressed by Equation 32, which is a function of the fuse diameter ϕ and length Lfuse.

$$\boldsymbol{\lambda = 4\phi L_{fuse}} \tag{32}$$

A value of slenderness equal to 60 is considered to avoid buckling during yielding in compression (Sarti et al., 2016), resulting in a fuse length of 165 mm for a fuse diameter of 11 mm. The two end sections of the devices are threaded and feature a larger diameter equal approximately to 1.3 diameter of the fuse (i.e., 14 mm). The anti-buckling steel tube has an external diameter of 2 times the larger diameter of the fuse-shaped bars, and it is filled with epoxy. These Plug&Play dissipaters are anchored to the beam through a tailored S275 steel plate (Detail B1 in) with two orders of fasteners: high-bond nails provide stiffness to the connection, while bolts provide strength. The nails are engaged under service conditions, and they are necessary to avoid significant displacement of the plate causing damage to timber. They are designed to provide sufficient stiffness and capacity to fully resist the shear force induced by the dissipaters, without considering also the contribution of the bolts. The latter, in fact, are engaged at the ultimate limit states. The connection is therefore designed to avoid damage up to the design earthquake, while accepting a certain degree of damage for earthquakes with higher intensity. All the rivets are placed at proper distances according to the aforementioned codes.

Funded by the European Union

This project has received funding from the European Union under the Horizon Europe Research & Innovation Programme (Grant Agreement no. 101123467 MultiCare). Views and opinions expressed are however those of author(s) only and do not necessarily reflect those of the European Union. Neither the European Union nor the granting authority can be held responsible for them.

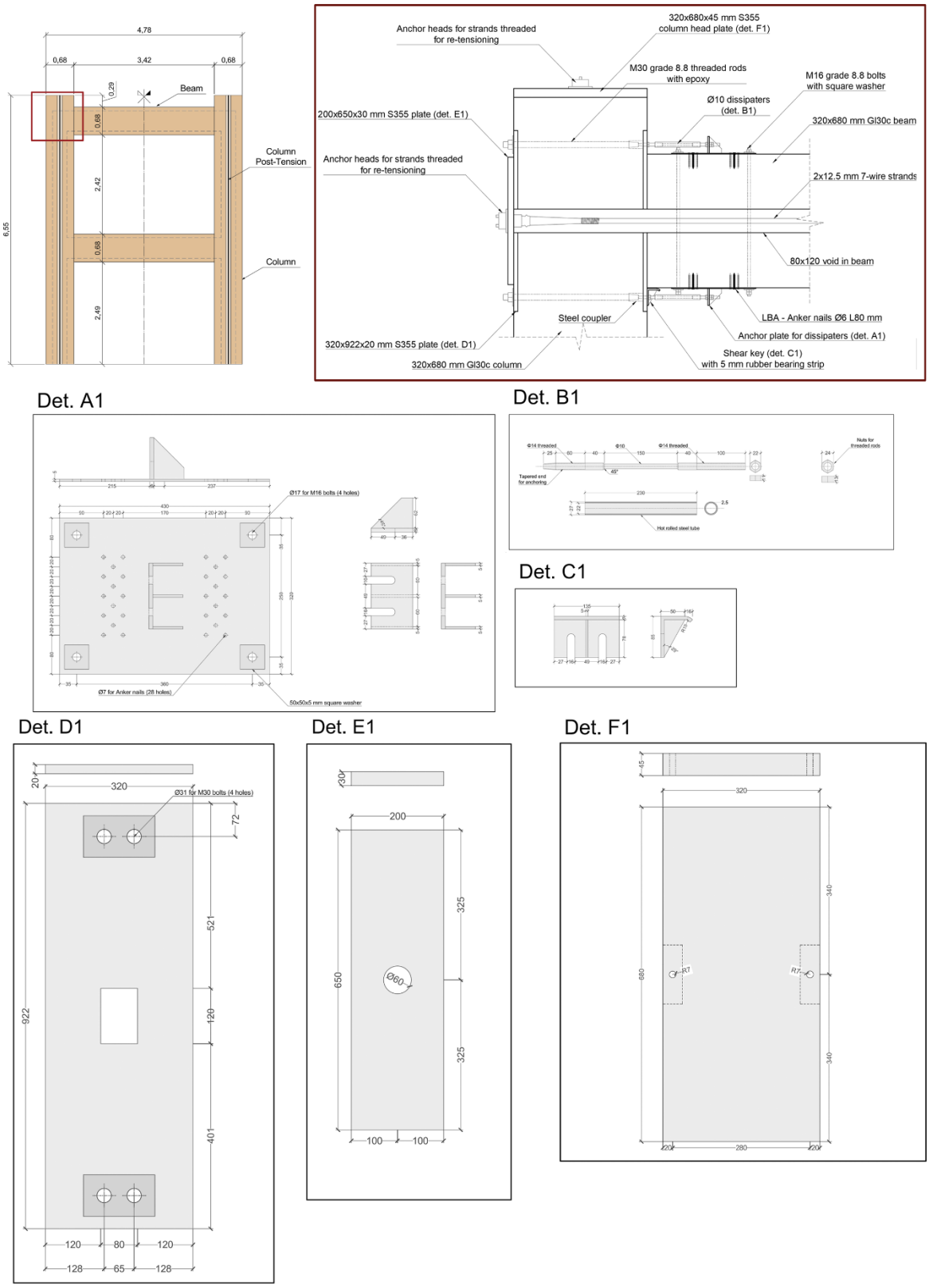

Figure 32. Example of a Pres-Lam exoskeleton and details of the beam-column joint.

This project has received funding from the European Union under the Horizon Europe Research & Innovation Programme (Grant Agreement no. 101123467 MultiCare). Views and opinions expressed are however those of author(s) only and do not necessarily reflect those of the European Union. Neither the European Union nor the granting authority can be held responsible for them.

The action on the anchoring plates in determined by Equation 33, representing the shear force induced by the Plug&Play devices, while the resistance of the plate is represented by the minimum between the shear resistance of the fasteners, the bearing resistance of the plate, and the tension resistance of the fasteners. Specifically, the most stringent verification is represented by the shear resistance, which is expressed by Equation 34 and Equation 35 for thin plates at single and double shear, respectively, or Equation 36 and Equation 37 for thick plates, depending on the diameters of the nails and the bolts.

$$V_{d,tot} = n_{diss}\left(\pi \frac{d_{fuse}^2}{4} f_{su}\right) \tag{33}$$

$$F_{v,Rk} = \min\begin{cases} 0.4 f_{h,k} t_1 d \\ 1.15\sqrt{2M_{y,Rk} f_{h,k} d} + \frac{F_{ax,Rk}}{4} \end{cases} \tag{34}$$

$$F_{v,Rk} = \min\begin{cases} 0.5 f_{h,2,k} t_2 d \\ 1.15\sqrt{2M_{y,Rk} f_{h,2,k} d} + \frac{F_{ax,Rk}}{4} \end{cases} \tag{35}$$

$$F_{v,Rk} = \min\begin{cases} f_{h,k} t_1 d\sqrt{2 + \frac{4M_{y,Rk}}{f_{h,k} d t_1^2}} - 1 + \frac{F_{ax,Rk}}{4} \\ 2.3\sqrt{M_{y,Rk} f_{h,k} d} + \frac{F_{ax,Rk}}{4} \\ f_{h,k} t_1 d \end{cases} \tag{36}$$

$$F_{v,Rk} = \min\begin{cases} 0.5 f_{h,2,k} t_2 d \\ 2.3\sqrt{2M_{y,Rk} f_{h,2,k} d} + \frac{F_{ax,Rk}}{4} \end{cases} \tag{37}$$

In the equations above n_{diss} is the number of dissipaters employed, d_{fuse} is the diameter of the dissipater fuse-shaped section, f_{su} is the ultimate tensile steel strength, $F_{v,Rk}$ is he characteristic shear resistance of the connection system, $f_{h,k}$ is the characteristic timber embedment strength, t_1 is the smaller length between the timber thickness and the length of fastener penetration, t_2 is the thickness of the timber element, d is the fastener diameter, $M_{y,Rk}$ is the characteristic yielding moment of the fastener, and $F_{ax,Rk}$ is its characteristic withdrawal resistance. In this example, given the size of the plates (i..e., 5 mm thick) and fasteners, the thin-plate verification criteria is applied to the bolts in double shear, while the thick-plate verification at single shear is used for the nails. From the calculation, 28 high-bond nails with a diameter of 6 mm and a length of 100 mm are needed, together with four M18 threaded roads instead of bolts. The effective shear resistance of the connection is given by Equation 38, considering the type of timber and the duration of load following the Italian and European Standards (EN 1995-1-1:2004, NTC 2018).

$$F_{v,Rd} = n_{eff} \frac{F_{v,Rk} k_{mod}}{\gamma_m} \tag{38}$$

Where, n_{eff} is the effective number of the fasteners used, which has to be calculated as a function of the distance in the load direction d_{rods} and the diameter ϕ_{rod}, if threaded rods are used in place of bolts as in this example (Equation 39); k_{mod} is the modification factor taking into account the effect of the duration of load and moisture content, which has been considered equal to 0.9 in the project (i.e., short-term load and standard moisture level); γ_m is the partial factor for material property considered equal to 1.3 for steel-timber connections.

Funded by the European Union

This project has received funding from the European Union under the Horizon Europe Research & Innovation Programme (Grant Agreement no. 101123467 MultiCare). Views and opinions expressed are however those of author(s) only and do not necessarily reflect those of the European Union. Neither the European Union nor the granting authority can be held responsible for them.

$$n_{eff} = min\left(n_{rods};\ n_{rods}^{0.9}\sqrt{\frac{d_{rods}}{13\emptyset_{rod}}}\right) \quad (39)$$

The dissipaters are bolted to a proper vertical plate welded to the horizontal one described above, which is designed to resist bending under the force coming from the dissipaters. Specifically, the moment resistance M_{Rd} of the plate is expressed by Equation (40) as function of the steel yielding strength $f_{y,p}$, the plate thickness t, and the length of the plate l_p (Figure 33).

$$M_{Rd} = \frac{0.9 f_{y,p} l_p t}{6} \quad (40)$$

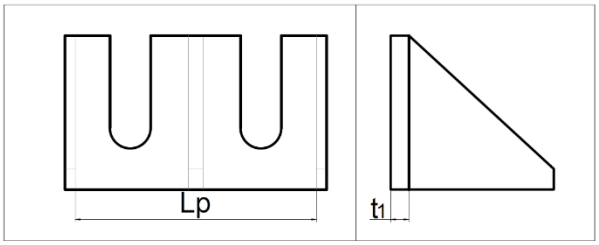

Figure 33. Detail of the vertical plate for the dissipaters anchoring.

As already mentioned in the previous paragraph, different shear transfer mechanism can be implemented in the design of Pres-Lam connections, e.g., considering the friction at the joint interface, or inserting a steel tube within the internal void containing the post-tensioned reinforcement. However, it is recommended not to rely on the first mechanism, as it fails in the unlikely event of a post-tensioning failure, while the second mechanism can cause damage to the beam during the rocking motion. For these reasons, in this example a steel corbel is designed as the designated shear key in the beam-column joint (Detail C1 in Figure 32). In order to avoid damage on timber during the gap opening, the corbel is bent at the end of the horizontal plate and a 5 mm rubber bearing strip is inserted between the timber beam and the corbel itself. Moreover, additional reinforcement plates are placed in the orthogonal direction to further increase the bending stiffness of the corbel. The verification proposed by the NZS are considered to make sure that the shear and moment resistance of the corbel is greater than the shear acting at the beam-column interface and the moment caused by the eccentricity at the centre of the horizontal plate. This type of shear key has proven its efficacy through a large shake table test conducted by Pampanin et al., 2023. The bearing and bending strength of the shear key are expressed through Equations 41 and 42, respectively:

$$V_{Rd} = \phi k_1 A_p f_{t,90} \quad (41)$$

$$M_{Rd} = \frac{\phi l_p t_p^2 f_{y,p}}{4} \quad (42)$$

This project has received funding from the European Union under the Horizon Europe Research & Innovation Programme (Grant Agreement no. 101123467 MultiCare). Views and opinions expressed are however those of author(s) only and do not necessarily reflect those of the European Union. Neither the European Union nor the granting authority can be held responsible for them.

Where, ϕ is the capacity factor which is equal to 0.9 for LVL and 0.8 for Glulam, k_1 is the modification factor for duration of load which is equal to 1 for a load combination consisting of permanent, earthquake and imposed action (NZS AS 1720.1:2022), A_p is the transversal section of the corbel, $f_{t,90}$ is the timber strength perpendicular to the grain, l_p is the length of the corbel section, t_p is its thickness, and $f_{y,p}$ is the steel yielding strength.
To reinforce the column in the perpendicular to grain direction, different details might be employed (see Figure 12). The best solution is to insert epoxied threaded rods in the column width (Figure 34a). The epoxy is particularly essential in the external joint to transfer compression within the joint and ensure the proper moment capacity, due to the presence of the beam on only one side of the joint. The rods diameter and the epoxy are verified against withdrawal following Equation 43, which represents the tension resistance of the system as the minimum between the steel rod tension resistance, the bond line resistance, and the adherent timber tension resistance.

$$F_{ax,Rd} = \min \begin{cases} f_{yd} A_{res} \\ \pi d l f_{v,d} \\ \pi d l f_{t,0,d} \end{cases} \quad (43)$$

In the Equation above, f_{yd} is the design yielding strength of the steel rod, d and l is the rod diameter and length, respectively, A_{res} is the relevant cross-section of the rod, $f_{t,o,d}$ is the design tension strength of timber, and $f_{v,d}$ is the design value of bond shear strength. The latter depends on the bond length of the steel rod, with higher values when shorter lengths are employed. The rods are jointed to the dissipaters coming from the beam by using a coupler (Figure 34b).

a)

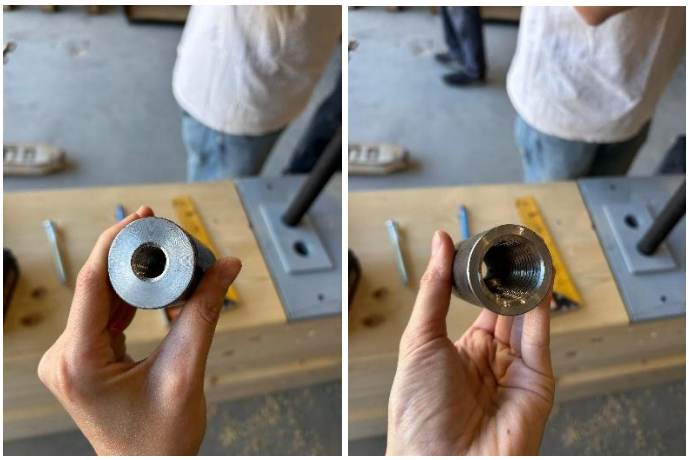

b)

Figure 34. a) Epoxied threaded rods passing through the column's width to reinforce the joint in the perpendicular to grain direction; b) A steel coupler used to joint the rods with the external Plug&Play dissipaters (pictures taken by the author).

The anchoring system for the beam's post-tensioning strands consists of two main plates: the first (i.e., the thinner one) acts as a reinforcement on the column against the perpendicular to grain action induced by the axial load of the tendons, while the second (i.e., the thicker one) is dimensioned as a flat plate simply supported at the edges with a concentrated central load coming from the post-tension (Figure 35). This is due to the fact that a central hole is present in both the plates, corresponding to the void within the beam and column to accommodate the tendons. The bending stress caused by the most external

Funded by the European Union

This project has received funding from the European Union under the Horizon Europe Research & Innovation Programme (Grant Agreement no. 101123467 MultiCare). Views and opinions expressed are however those of author(s) only and do not necessarily reflect those of the European Union. Neither the European Union nor the granting authority can be held responsible for them.

plate (detail E1 in Figure 32) on the first plate (detail D1 in Figure 32) when a post-tensioning action is present at the centre is given by Equation 44. This stress must be lower than the steel strength; in this example a steel S355 type is considered.

$$\sigma = \frac{1.5P}{\pi t^2}\left((1+\nu)\ln\left(\frac{2b}{\pi e}\right)+k\right) \tag{44}$$

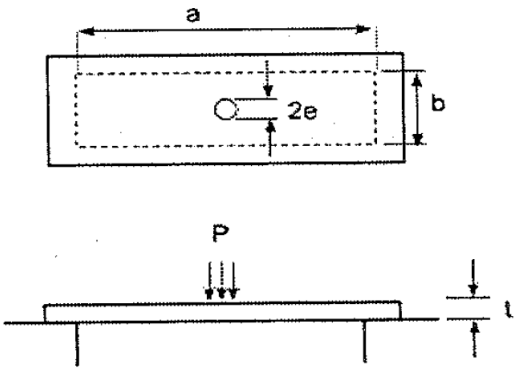

Figure 35. Simply supported plate with concentrated load at centre.

In Equation 44 P is the post-tensioning force, t is the external plate thickness, ν is the Poisson ratio which is considered equal to 0.3 for steel, b is the shorter dimension of the first hole (detail D1 in Figure 32), k is a coefficient depending on the aspect ratio of the first hole (Table 16), and e is given by Equation 45 as a function of the plate thickness t and the second hole's radius c.

$$e = \begin{cases} \left(\sqrt{1.6c^2+t^2}\right) - 0.675t \; if \; e < 0.5t \\ c \; if \; e \geq 0.5t \end{cases} \tag{45}$$

Table 16. Value of coefficient k_2 (NZS 3404:1997).

	a/b								
	1.0	1.1	1.2	1.4	1.6	1.8	2.0	3.0	≥4
k	0.435	0.565	0.650	0.789	0.875	0.927	0.958	1.000	0.000

Finally, the column head plate is designed (detail F1 in Figure 32) to resist the post-tensioning force transmitted by the strands within the column. The required plate thickness is determined by evaluating the bending moment generated by the force acting at the center of the plate's opening, through which the post-tensioned strands pass. For the portion of the plate corresponding to the cut-out in the timber section, a corbel-type static scheme is adopted. The resisting moment is provided by the plate's cross-section along the shorter direction of the cut-out.

5.2.2. Column-foundation joint design

The column-foundation connection follows, illustrated in Figure 36, follows the same rules of the beam-column joint as far as the dissipaters anchoring plates are concerned. In this case, however, the shear key consists of a base plate turning vertically – in this design example for 50 mm – on the column. The friction at the timber-steel interface acts as the shear mechanism. The tension on the vertical plate area – determined by the effective shear at the base column which is the seismic base shear minus the friction shear contribution as a function of the friction coefficient between steel and timber, typically equal to 0.4, and the axial load – has to be lower than the timber shear strength. Additionally, the tension

This project has received funding from the European Union under the Horizon Europe Research & Innovation Programme (Grant Agreement no. 101123467 MultiCare). Views and opinions expressed are however those of author(s) only and do not necessarily reflect those of the European Union. Neither the European Union nor the granting authority can be held responsible for them.

given by the bending moment resulting from timber pressure on the shear key must be lower than the steel yielding strength.

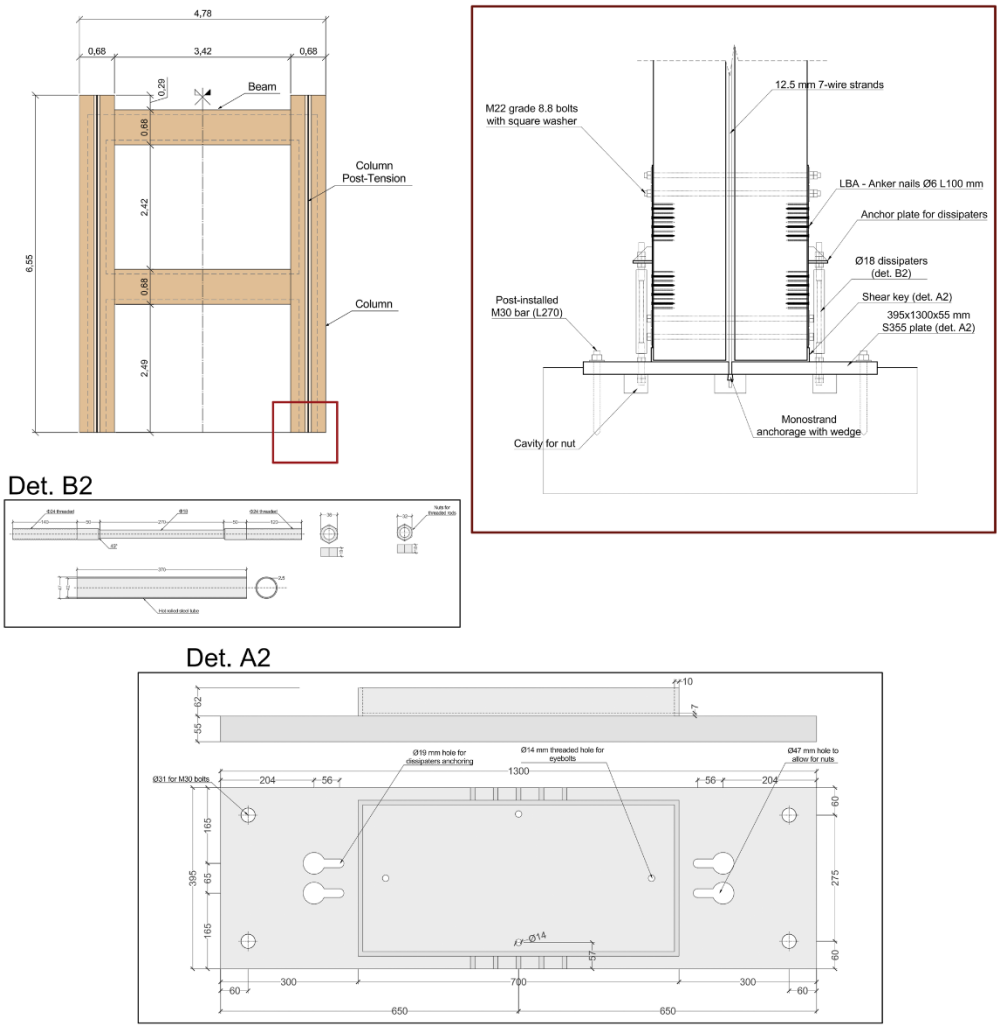

Figure 36. Column to foundation joint and details of the base plate.

Below the shear key, a thicker plate (Detail A2 in Figure 36) is installed and dimensioned to resist bending against the force induced by the dissipaters (Detail B2 in Figure 36) and the post-tensioning, which are connected to the plate. Specifically, a simple beam static scheme is applied (Figure 37), where the vertical forces induced by the dissipaters and the post-tensioning tendons must be resisted by a proper plate section (i.e., thickness) and proper anchors – either pre or post-installed - within the concrete foundation. A slotted hole is provided for anchoring the Plug&Play dissipaters, in order to allow them to be inserted into the plate, then placed in the correct position, and finally bolted to the plate. A cavity left within the concrete foundation is needed to secure both the dissipaters and the post-tensioning tendons.
It is important to note that different base plate configurations can be used for Pres-Lam post-tensioned columns; therefore, designer must select the appropriate verification method based on the plate adopted.

Funded by the European Union

This project has received funding from the European Union under the Horizon Europe Research & Innovation Programme (Grant Agreement no. 101123467 MultiCare). Views and opinions expressed are however those of author(s) only and do not necessarily reflect those of the European Union. Neither the European Union nor the granting authority can be held responsible for them.

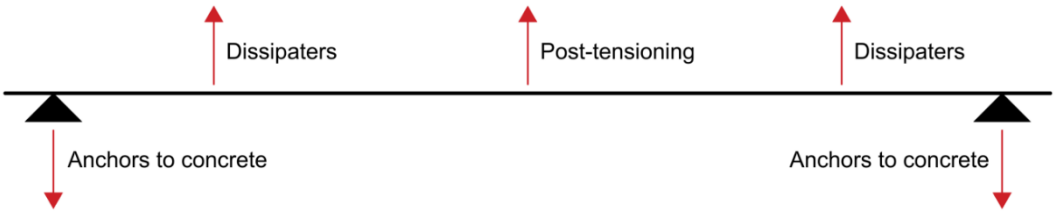

Figure 37. Static scheme adopted to design the base plate for the post-tensioned columns.

5.2.3. Exoskeleton connection to the existing structure

The connection between the existing beam and the Pres-Lam beam is the structural element responsible for transferring seismic forces and for correctly activating the exoskeleton function.

The chosen connection consists of a post-installed threaded rod anchored into the concrete using chemical resin (HYB-FIX Rothoblaas). The rod is connected to the exoskeleton through a steel plate screwed onto the timber beam by means of partially threaded screws for plates, such as HBS PLATE Rothoblaas. To avoid excessive play and to stiffen the rod, a specially designed thick washer has been bolted to the plate.

Therefore, the structural components of the connection to be verified are:

- Yielding and shear failure of the steel elements;
- Anchorage resistance on the concrete side;
- Plate-to-timber connection with screws.

With regard to the steel plate and washer, in order to avoid excessive deformations, relatively large thicknesses were adopted, carefully verified also in terms of resistance. For this reason, this aspect will not be further investigated here.

One of the governing resistance modes is the failure of the steel connector under bending action, due to the presence of a lever arm, in this case equal to 40 mm. The existence of a "gap" introduces a weakness for the rod and can amplify yielding compared to a standard configuration without lever arm.

The design of post-installed fasteners in concrete follows EN 1992-4:2018. In particular, checks for post-installed fasteners subjected to shear are reported in §7.2.2 of the code, and the failure modes are illustrated in Figure 38.

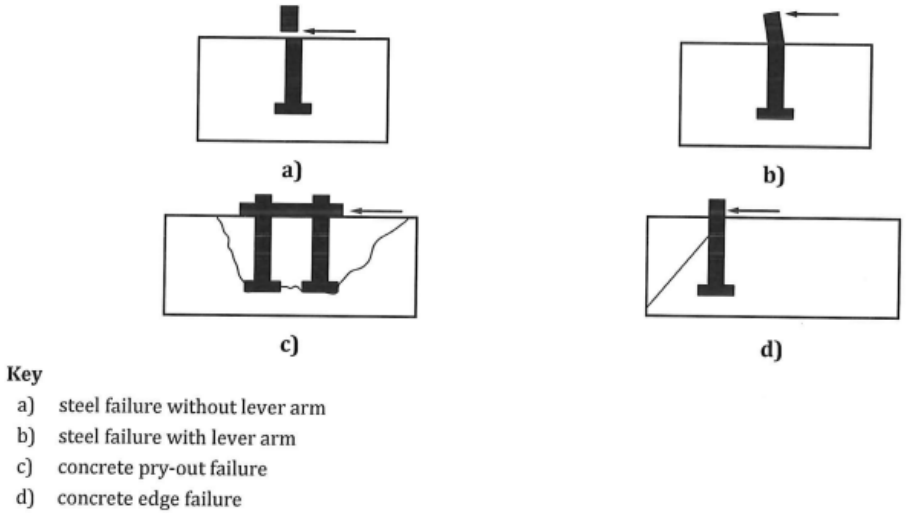

Figure 38. Failure modes of post-installed fasteners in concrete.

This project has received funding from the European Union under the Horizon Europe Research & Innovation Programme (Grant Agreement no. 101123467 MultiCare). Views and opinions expressed are however those of author(s) only and do not necessarily reflect those of the European Union. Neither the European Union nor the granting authority can be held responsible for them.

In case (b), steel failure by yielding, the design resistance is calculated according to Equation 46:

$$V_{Rk,s,M} = \frac{\alpha_M \cdot M_{Rk,s}}{l_a} \quad (46)$$

Where:

- α_M is the factor accounting for the degree of restraint of the fastener at the side of the fixture of the application in question. In this study, it is conservatively set equal to 1, assuming no rotational restraint.
- $l_a = a_3 + e_1$ (Figure 39)
- a_3 = half of the nominal diameter of the threaded rod
- e_1 = lever arm, here equal to 40 mm
- $M_{Rk,s} = M^0_{Rk,s} \cdot (1 - \frac{N_{Ed}}{N_{Rd,s}})$
- $N_{Rd,s} = N_{Rk,s}/\gamma_{Ms}$

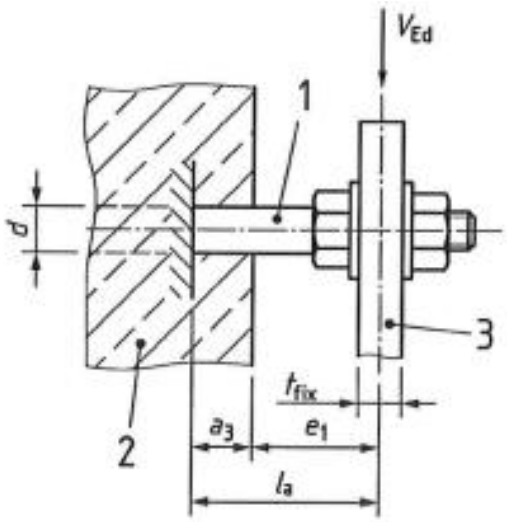

Figure 39. Geometry parameters of the proposed connection.

This verification ensures the resistance of the threaded rod.
On the concrete side, the main check concerns the concrete pry-out failure. In accordance with Eurocode 2, Equations 47 and 48 apply:

$$V_{Rd,cp} = \frac{V_{Rk,cp}}{\gamma_{Ms}} \quad (47)$$

$$V_{Rk,cp} = k_8 \cdot N_{Rk,c} \quad (48)$$

Where $N_{Rk,c}$ is the characteristic concrete cone resistance, calculated according to §7.2.1.4 in the Eurocode, considering only a shear force.
Since the formula is rather complex, it is not reported here and reference should be made to the code. At an operational level, the post-installed resin anchor has been evaluated

This project has received funding from the European Union under the Horizon Europe Research & Innovation Programme (Grant Agreement no. 101123467 MultiCare). Views and opinions expressed are however those of author(s) only and do not necessarily reflect those of the European Union. Neither the European Union nor the granting authority can be held responsible for them.

using the software “MY PROJECT CONCRETE ANCHORS”, where geometry and loads were modelled to derive the design check (Figure 40).
The design shear force to be transferred is 150 kN. To avoid an excessive reduction of connection resistance due to seismic design rules, the load has been considered as quasi-static. A total of 8 anchors were adopted, each designed to resist 25 kN.
To properly account for group effects, the model included a 40 mm thick steel plate to simulate the gap (already verified manually), with two anchors loaded at 50 kN each. This allowed both single-anchor shear resistance and group effects to be automatically verified.

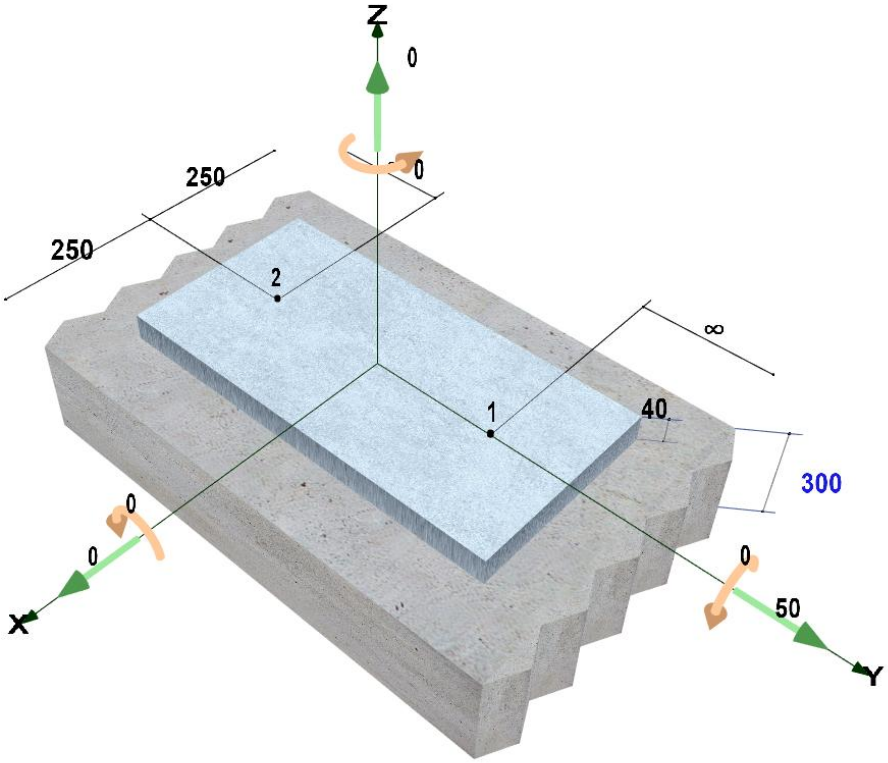

Figure 40. Connection geometry modelled within the software.

Finally, the last check concerns the thick plate-to-timber connection with HBS PLATE screws. The design is performed in accordance with EN 1995-1-1:2004+A1:2008, using the following Equation 49:

$$F_{v,Rk} = min \begin{cases} f_{h,k}\ x\ t_1 x\ d \\ f_{h,k}\ x\ t_1 x\ d\ x\ [\sqrt{2 + \frac{4\ x\ M_{y,Rk}}{f_{h,k}\ x\ t_1^2 x\ d}} - 1] + F_{ax,Rk}/4 \\ 2.3\sqrt{M_{y,Rk} x f_{h,k} x d} + F_{ax,Rk}/4 \end{cases} \quad (49)$$

The parameters are analogous to those already presented in Chapter 4.1, while for the characteristic embedment strength reference is made to the specific ETA of the HBS PLATE screws (ETA 11/0030).
The connection is verified with 6 HBS PLATE 12x120 mm screws, and the calculation can also be carried out analytically using the software “MY PROJECT”.

Funded by the European Union

This project has received funding from the European Union under the Horizon Europe Research & Innovation Programme (Grant Agreement no. 101123467 MultiCare). Views and opinions expressed are however those of author(s) only and do not necessarily reflect those of the European Union. Neither the European Union nor the granting authority can be held responsible for them.

6. References

Brown, A., Lester, J., Pampanin, S., Pietra, D. (2012). Pres-Lam in practice: A damage-limiting rebuild project. In Proceedings of the SESOC New Zealand Conference.

Christopoulos, C., Filiatrault, A., Uang, C.M., Folz, B. (2002). Posttensioned energy dissipating connections for moment-resisting steel frames. Journal of Structural Engineering, 128(9), 1111-1120.

Cosenza, E., Del Vecchio, C., Di Ludovico, M., Dolce, M., Moroni, C., Prota, A., Renzi, E., (2018). The Italian Guidelines for Seismic Risk Classification of Constructions: Technical Principles and Validation. Bulletin of Earthquake Engineering 16 (12), 5905–35.

D'Amore, S., & Pampanin, S. (2025). Displacement-based seismic retrofit of reinforced concrete buildings through low-damage exoskeletons. Engineering Structures, 322, 119209.

Davies, M., Fragiacomo, M. (2011). Long-term behavior of prestressed LVL members. I: Experimental tests. Journal of Structural Engineering, 137(12), 1553-1561.

De Luca, F., Woods, G. E., Galasso, C., & D'Ayala, D. (2018). RC infilled building performance against the evidence of the 2016 EEFIT Central Italy post-earthquake reconnaissance mission: empirical fragilities and comparison with the FAST method. Bulletin of Earthquake Engineering, 16, 2943-2969.

Decanini LD, De Sortis A, Goretti A, Liberatore L, Mollaioli F, Bazzurro P. Performance of reinforced concrete buildings during the 2002 Molise, Italy, earthquake. Earthquake Spectra 2004; 20(SPEC. 1). DOI: 10.1193/1.1765107.

Di Cesare A, Ponzo FC, Nigro D, Pampanin S, Smith T. Shaking table testing of post-tensioned timber frame building with passive energy dissipation systems. *Bulletin of Earthquake Engineering* 2017; 15(10): 4475–4498. DOI: 10.1007/s10518-017-0115-9.

Di Trapani F, Bogatkina V, Petracca M, Camata G. Evaluation of the additional shear demand due to frame-infill interaction: a new capacity model. Procedia Structural Inte-grity 2023; 44: 496–503. DOI: 10.1016/J.PROSTR.2023.01.065.

EN 1992-4:2018 (2018). Eurocode 2: Design of concrete structures – Part 4: Design of fastenings for use in concrete. Brussels, Belgium.

EN 1993-1-8 (2005): Eurocode 3: Design of steel structures - Part 1-8: Design of joints. Brussels, Belgium.

EN 1995-1-1 (2004): Eurocode 5: Design of timber structures - Part 1-1: General - Common rules and rules for buildings. Brussels, Belgium.

ETA TR 070 (2019). European Organisation for Technical Assessment – Technical Report: Design of Glued-in Rods for Timber Connections. Brussels, Belgium.

Fédération internationale du béton, fib. (2003). Seismic Design of Precast Concrete Building Structures: State-of-the-art Report.

Gkatzogias, K., Pohoryles, D. A., Romano, E., Veljkovic, A., Dimova, S., Tsionis, G., ... & Sousa, M. (2022, September). A Pilot Project on the Integrated Seismic and Energy Retrofit of European Buildings. In Proceedings of the Third European Conference on Earthquake Engineering and Seismology—3ECEES, Bucharest, Romania (pp. 4-9).

Funded by the European Union

This project has received funding from the European Union under the Horizon Europe Research & Innovation Programme (Grant Agreement no. 101123467 MultiCare). Views and opinions expressed are however those of author(s) only and do not necessarily reflect those of the European Union. Neither the European Union nor the granting authority can be held responsible for them.

Granello G, Leyder C, Palermo A, Frangi A, Pampanin S. Design Approach to Predict Post-Tensioning Losses in Post-Tensioned Timber Frames. *Journal of Structural Engineering* 2018; 144(8). DOI: 10.1061/(asce)st.1943-541x.0002101.

Granello, G., Giorgini, S., Palermo, A., Carradine, D., Pampanin, S., Finch, R. (2017). Long-term behavior of LVL posttensioned timber beams. Journal of Structural Engineering, 143(12), 04017158.

Granello, G., Palermo, A., Pampanin, S., Pei, S., Van De Lindt, J. (2020). Pres-lam buildings: state-of-the-art. Journal of Structural Engineering, 146(6), 04020085.

Granello, G., Palermo, A., Pampanin, S., Smith, T., Sarti, F. (2018). The implications of post-tensioning losses on the seismic response of Pres-Lam frames. Bulletin of the New Zealand Society for Earthquake Engineering, 51(2), 57-69.

Holden, T., Devereux, C., Haydon, S., Buchanan, A., Pampanin, S. (2016). NMIT Arts & Media Building—Innovative structural design of a three storey post-tensioned timber building. Case studies in structural engineering, 6, 76-83.

Horne, P.D., Palermo, A.A., Abu, A.K., Moss, P.J. (2022). Challenges of seismic detailing on the fire performance of post-tensioned timber frames. Bulletin of the New Zealand Society for Earthquake Engineering, 55(4), 229-240.

Iqbal, A., Pampanin, S., Buchanan, A.H. (2016). Seismic performance of full-scale post-tensioned timber beam-column connections. Journal of earthquake engineering, 20(3), 383-405.

Marriott, D., Pampanin, S., Bull, D., & Palermo, A. (2008). Dynamic testing of precast, post-tensioned rocking wall systems with alternative dissipating solutions.

Miliziano, A. (2019). Seismic performance of low-damage post-tensioned timber frame systems. Master Thesis. Sapienza University of Rome, Rome, Italy.

NTC (2018). D.M. del Ministero delle Infrastrutture e dei trasporti del 17/01/2018. Aggiornamento delle Norme Tecniche per le Costruzioni (NTC 2018), Italy.

Molitierno C, Del Vecchio C, Di Ludovico M, Prota A. Pseudodynamic Tests and Numerical Modelling for Damage Analysis of Infilled RC Frames. Journal of Earthquake Engineering 2023; 27(16): 4549–4574. DOI: 10.1080/13632469.2023.2183048.

Moroder, D., Smith, T., Dunbar, A., Pampanin, S., Buchanan, A. (2018). Seismic testing of post-tensioned Pres-Lam core walls using cross laminated timber. Engineering Structures, 167, 639-654.

New Zealand Concrete Society, NZCS. (2010). PRESSS Design Handbook. Wellington, New Zealand.

New Zealand Society for Earthquake Engineering, NZSEE. (2017). The Seismic Assessment of Existing Buildings - Technical Guidelines for Engineering Assessments. Wellington, New Zealand.

Newcombe, M.P., Pampanin, S., Buchanan, A.H. (2010). Global response of a two storey Pres-Lam timber building. In Proceedings of the 2010 NZSEE Conference, Wellington, New Zealand.

Funded by the European Union

This project has received funding from the European Union under the Horizon Europe Research & Innovation Programme (Grant Agreement no. 101123467 MultiCare). Views and opinions expressed are however those of author(s) only and do not necessarily reflect those of the European Union. Neither the European Union nor the granting authority can be held responsible for them.

NZS 3404 (1997). Standards New Zealand: Steel Structures Standard – Parts 1 and 2. Wellington, New Zealand.

NZS AS 1720.1 (2022). New Zealand Standard: Timber Structures – Part 1:Design methods. Wellington, New Zealand.

Palermo, A, Pampanin, S, Buchanan, A, Newcombe, M. (2005). Seismic design of multi-storey buildings using laminated veneer lumber (LVL). In Proceedings of the NZSEE Conference, Taupo, New Zealand.

Palermo, A, Pampanin, S, Buchanan, A. (2006). Experimental investigations on LVL seismic resistant wall and frame subassemblies. In Proceedings of the 1st ECEES Conference, Geneva, Italy.

Palermo, A., Pampanin, S., Fragiacomo, M., Buchanan, A.H., Deam B. L. (2006). Innovative Seismic Solutions for Multi-storey LVL Timber Buildings. In Proceedings of the 9th World Conference on Timber Engineering, Portland, OR.

Pampanin, S, Palermo, A, Buchanan, A.H. (2013). Design Guide Australia and New Zealand - Post-Tensioned Timber Buildings. Structural Timber Innovation Company (STIC), Christchurch, New Zealand.

Pampanin, S. (2006). Controversial aspects in seismic assessment and retrofit of structures in modern times: Understanding and implementing lessons from ancient heritage. Bulletin of the New Zealand Society for Earthquake Engineering, 39,120–134.

Pampanin, S. (2010). PRESSS Design Handbook. NZ Concrete Society.

Pampanin, S. (2012). Reality-check and renewed challenges in earthquake engineering: implementing low-damage structural systems – from theory to practice. Bulletin of New Zealand Society for Earthquake Engineering, 45(4), 137–160.

Pampanin, S. (2015). Towards the “Ultimate Earthquake-Proof” Building: Development of an Integrated Low-Damage System. Perspectives on European Earthquake Engineering and Seismology, 2, 321-358.

Pampanin, S., Ciurlanti, J., Bianchi, S., Perrone, D., Granello, G., Palmieri, M., Grant, D.N., Palermo, A., Costa, A.C., Candeias, P.X., Correia, A.A. (2023). Triaxial shake table testing of an integrated low-damage building system. Earthquake Engineering & Structural Dynamics, 52(10), 2983-3007.

Pampanin, S., Magenes, G., Carr, A. (2003). Modelling of shear hinge mechanism in poorly detailed RC beam-column joints. In proceedings of fib 2003 Symposium "Concrete Structures in Seismic Regions”. Athens, Greece.

Pampanin, S., Priestley, M.N., Sritharan, S. (2001). Analytical modelling of the seismic behaviour of precast concrete frames designed with ductile connections. Journal of Earthquake Engineering, 5(03), 329-367.

Panagiotakos TB, Fardis MN. Seismic Response of infilled RC Frames Structures. 11th world Conference on Earthquake Engineering.

Park, R., Paulay, T. (1975). Reinforced Concrete Structures. John Wiley & Sons. New York.
Priestley, M. N., & Tao, J. R. (1993). Seismic response of precast prestressed concrete frames with partially debonded tendons. PCI journal, 38(1), 58-69.

Funded by the European Union

This project has received funding from the European Union under the Horizon Europe Research & Innovation Programme (Grant Agreement no. 101123467 MultiCare). Views and opinions expressed are however those of author(s) only and do not necessarily reflect those of the European Union. Neither the European Union nor the granting authority can be held responsible for them.

Priestley, M.J.N. (1991). Overview of PRESSS Research Program. PCI Journal, 36(4), 50–57.

Priestley, M.J.N., Sritharan, S., Conley, J.R., Pampanin, S. (1999). Preliminary Results and Conclusions from the PRESSS Five-Story Precast Concrete Test Building. PCI Journal, 44(6), 42–67.

Priestley, M.J.N. (2002). Direct displacement-based design of precast/prestressed concrete buildings. PCI Journal, 47(6), 66-79.

Priestley, M.J.N., Calvi, G.M., Kowalsky, M.J. (2007). Displacement-Based Seismic Design of Structures. Earthquake Spectra, 24(2), 555–557.

Ruaumoko Solutions (2012) St Elmo Courts Rebuild: Design features report, Christchurch, New Zealand.

Sarti, F., Palermo, A., Pampanin, S. (2016). Fuse-type external replaceable dissipaters: Experimental program and numerical modelling. Journal of Structural Engineering, 142(12), 04016134.

Sarti, F., Palermo, A., Pampanin, S. (2016). Quasi-static cyclic testing of two-thirds scale unbonded posttensioned rocking dissipative timber walls. Journal of Structural Engineering, 142(4), E4015005.

Sause, R., Ricles, J.M., Roke, D., Seo, C. Y., Lee, K.S. (2006). Design of self-centring steel concentrically-braced frames. In Proceedings from the 4th International Conference on Earthquake Engineering.

Smith T, Ponzo FC, Di Cesare A, Pampanin S, Carradine D, Buchanan AH, *et al.* Post-tensioned glulam beam-column joints with advanced damping systems: Testing and numerical analysis. *Journal of Earthquake Engineering* 2014; 18(1): 147–167. DOI: 10.1080/13632469.2013.835291.

Smith, T. (2014). Post-tensioned Timber Frames with Supplemental Damping Devices. PhD thesis, University of Canterbury, Christchurch, New Zealand.

Smith, T., Carradine, D.M., Pampanin, S., Ditommaso, R., Ponzo, F.C. (2012). Seismic performance of a post-tensioned LVL building subjected to the Canterbury earthquake sequence. In Proceedings of the 2012 NZSEE Conference.

van Beerschoten, W. (2013). Structural performance of post-tensioned timber frames under gravity loading. PhD Thesis, University of Canterbury, New Zealand.

van Beerschoten, W., Smith, T., Palermo, A., Pampanin, S., Ponzo, F. C. (2011). The stiffness of beam to column connections in post-tensioned timber frames.

Wanninger, F., Frangi, A., Fragiacomo, M. (2014). Long-term behavior of posttensioned timber connections. Journal of Structural Engineering, 141(6), 04014155.

Funded by the European Union

This project has received funding from the European Union under the Horizon Europe Research & Innovation Programme (Grant Agreement no. 101123467 MultiCare). Views and opinions expressed are however those of author(s) only and do not necessarily reflect those of the European Union. Neither the European Union nor the granting authority can be held responsible for them.